

## $Z \sim 7 - 10$ GALAXIES IN THE HUDF AND GOODS FIELDS, AND THEIR UV LUMINOSITY FUNCTIONS

RYCHARD J. BOUWENS<sup>2</sup>, GARTH D. ILLINGWORTH<sup>2</sup>, MARIJN FRANX<sup>3</sup>, HOLLAND FORD<sup>4</sup>

<sup>1</sup> Based on observations made with the NASA/ESA Hubble Space Telescope, which is operated by the Association of Universities for Research in Astronomy, Inc., under NASA contract NAS 5-26555. These observations are associated with programs #7235, 7817, 9425, 9575, 9797, 9803, 9978, 9979, 10189, 10339, 10340, 10403, 10530, 10632, 10872, and 11082. Observations have been carried out using the Very Large Telescope at the ESO Paranal Observatory under Program ID(s): LP168.A-0485. Based in part on data collected at the Subaru Telescope and obtained from SMOKA, which is operated by the Astronomy Data Center, National Astronomical Observatory of Japan.

<sup>2</sup> Astronomy Department, University of California, Santa Cruz, CA 95064

<sup>3</sup> Leiden Observatory, Postbus 9513, 2300 RA Leiden, Netherlands and

<sup>4</sup> Department of Physics and Astronomy, Johns Hopkins University, 3400 North Charles Street, Baltimore, MD 21218

*Draft version October 25, 2018*

### ABSTRACT

We use all available deep optical ACS and near-IR data over both the HUDF and the two GOODS fields to search for star-forming galaxies at  $z \gtrsim 7$  and constrain the  $UV$  LF within the first 700 Myrs. Our data set includes  $\sim 23$  arcmin<sup>2</sup> of deep NICMOS  $J+H$  data and  $\sim 248$  arcmin<sup>2</sup> of ground-based (ISAAC+MOIRCS) data, coincident with ACS optical data of greater or equal depths. In total, we find  $8 \langle z \rangle \sim 7.3$   $z$ -dropouts in our search fields, but no  $z \sim 9$   $J$ -dropout candidates. A careful consideration of a wide variety of different contaminants suggest an overall contamination level of just  $\sim 12\%$  for our  $z$ -dropout selection. After performing detailed simulations to accurately estimate the selection volumes, we derive constraints on the UV LFs at  $z \sim 7$  and  $z \sim 9$ . For a faint-end slope  $\alpha = -1.74$ , our most likely values for  $M_{UV}^*$  and  $\phi^*$  at  $z \sim 7$  are  $-19.8 \pm 0.4$  mag and  $1.1_{-0.7}^{+1.7} \times 10^{-3}$  Mpc<sup>-3</sup>, respectively. Our search results for  $z \sim 9$   $J$ -dropouts set a  $1\sigma$  lower limit on  $M_{UV}^*$  of  $-19.6$  mag assuming that  $\phi^*$  and  $\alpha$  are the same as their values at slightly later times. This lower limit on  $M_{UV}^*$  is 1.4 mag fainter than our best-fit value at  $z \sim 4$ , suggesting that the  $UV$  LF has undergone substantial evolution over this time period. No evolution is ruled out at 99% confidence from  $z \sim 7$  to  $z \sim 6$  and at 80% confidence from  $z \sim 9$  to  $z \sim 7$ . The inferred brightening in  $M_{UV}^*$  with redshift (i.e.,  $M_{UV}^* = (-21.02 \pm 0.09) + (0.36 \pm 0.08)(z - 3.8)$ ) matches the evolution expected in the halo mass function, if the mass-to-light ratio of halos evolves as  $\sim (1+z)^{-1}$ . Finally, we consider the shape of the  $UV$  LF at  $z \gtrsim 5$  and discuss the implications of the Schechter-like form of the observed LFs, particularly the unexpected abrupt cut-off at the bright end.

*Subject headings:* galaxies: evolution — galaxies: high-redshift

### 1. INTRODUCTION

One of the most important goals of observational cosmology has been to identify galaxies at the earliest times and to characterize their evolution. Over the past few years, substantial progress has been made on this front, particularly at high redshifts ( $z \sim 4 - 6$ ). Much of this progress has been due to the significant quantity of deep multi-wavelength data made possible by instruments like the Hubble Space Telescope (HST) Advanced Camera for Surveys (Ford et al. 2003) or Subaru's Suprime-Cam (Miyazaki et al. 2002). As a result, current selections (e.g., Yoshida et al. 2006; Beckwith et al. 2006; Bouwens et al. 2007) now number in the tens of thousands of galaxies and reach to luminosities as faint as  $-16$  AB mag ( $\sim 0.01 L_{z=3}^*$ ). This has enabled astronomers to measure a wide-range of properties in high-redshift galaxies and examine their evolution across cosmic time.

One of the key observables considered in previous studies of high-redshift galaxies is the luminosity function in the rest-frame  $UV$ . The  $UV$  LF is of significant interest not only because of the quantitative constraints it imposes on early galaxy formation, but also because of the information it provides on the star formation rate and  $UV$  output of galaxies at the earliest times. This latter information is important for investigating the role galaxies may have played in the reionization of the universe

(e.g., Stanway et al. 2003; Giavalisco et al. 2004b; Yan & Windhorst 2004; Bouwens et al. 2006).

In principle, the large statistical samples of star-forming galaxies at  $z \sim 4 - 6$  just described allow us to determine the  $UV$  LFs and their evolution in great detail out to  $z \sim 6$ . Unfortunately, despite the large sample sizes and wide luminosity ranges of current selections, there continues to be some uncertainty regarding how the  $UV$  LF evolves at very high redshift (i.e., from  $z \gtrsim 6$  to  $z \sim 3$ ). Some groups (Shimasaku et al. 2005; Bouwens et al. 2006; Yoshida et al. 2006; Ouchi et al. 2004a; Bouwens et al. 2007; Dickinson et al. 2004) have argued the evolution occurs primarily at bright end of the LF, others (Iwata et al. 2003; Sawicki & Thompson 2006; Iwata et al. 2007) have asserted it happens more at the faint-end, and still others have suggested the evolution is independent of luminosity (Beckwith et al. 2006). The diversity of conclusions drawn by different teams would seem to suggest that systematics are likely playing a large role. A careful discussion of this issue as well as detailed comparisons with contemporary determinations of the  $UV$  LF at  $z \sim 4 - 6$  can be found in Bouwens et al. (2007).

One way of gaining additional leverage in looking at the evolution of the  $UV$  LF at high redshift is to push to even higher redshift, i.e.,  $z \sim 7 - 10$ , to see what

galaxies were like at these epochs. Since it is expected that changes in the  $UV$  LF will be much more substantial over the interval  $z \sim 7 - 10$  to  $z \sim 3 - 4$  than from  $z \sim 6$  to  $z \sim 4$ , it should be relatively easy to ascertain how the  $UV$  LF is evolving at early cosmic times. The challenge, of course, is that the number of star-forming galaxy candidates at  $z \sim 7 - 10$  has been very small, of order  $\sim 4 - 5$  galaxies (Bouwens et al. 2004c; Bouwens et al. 2005; Bouwens & Illingworth 2006; Iye et al. 2006; Labbé et al. 2006; Mannucci et al. 2007; Stark et al. 2007b; Bradley et al. 2008). As a result, the bulk of the effort has been directed towards simply establishing the overall prevalence of bright star-forming galaxies at  $z \sim 7 - 10$  (Bouwens et al. 2004c; Yan & Windhorst 2004; Bouwens et al. 2005; Bouwens & Illingworth 2006; Mannucci et al. 2007; Iye et al. 2006; Stanway et al. 2008).

In the present work, we will try to take studies of the  $UV$  LF at  $z \gtrsim 7$  one step further and not just look at the overall prevalence of star-forming galaxies at  $z \gtrsim 7$ , but at how the volume density of these galaxies appears to vary as a function of luminosity. In doing so, we will attempt to derive constraints on the overall shape of the  $UV$  LF at  $z \gtrsim 7$  and therefore evaluate different models for how the  $UV$  LF evolves with cosmic time. In particular, we are interested in looking at how the volume density of the bright population evolves and how this compares to the evolution of the faint population. If the mean luminosity of galaxies really does increase with time at early cosmic times, as one might expect from hierarchical models, the volume density of bright galaxies should evolve much more rapidly at  $z \gtrsim 7$  than the volume density of the faint population. This change has been alternatively parametrized as a brightening of the characteristic luminosity  $M_{UV}^*$  with cosmic time (e.g., Bouwens et al. 2006; Yoshida et al. 2006; Bouwens et al. 2007) or a flattening of the faint-end slope  $\alpha$  (e.g., Yan & Windhorst 2004).

To help with this endeavor, we will make use of the previous data used by our group in high-redshift ( $z \sim 7 - 10$ ) galaxy searches (e.g., Bouwens & Illingworth 2006; Bouwens et al. 2005) and also take advantage of a significant amount of newer data. Among these new data are deep ACS observations over the NICMOS parallels to the HUDF (Oesch et al. 2007), a large number of moderately deep NICMOS observations over the two GOODS fields (H. Teplitz et al. 2008, in prep), the deep wide-area ISAAC observations over the CDF-South GOODS field (Mannucci et al. 2007; Stanway et al. 2008; B. Vandame et al. 2008, in preparation; J. Retzlaff et al. 2008, in prep), and the deep wide-area MOIRCS observations over the HDF-North GOODS field (Kajisawa et al. 2006; Ouchi et al. 2007). We will also be taking advantage of improvements in our NICMOS reduction techniques to push our previous selections slightly fainter. These new data (particularly the new wide-area ground-based data) will be crucial for examining the  $UV$  LF at  $z \gtrsim 7$  over a wider range in luminosity than was possible in previous work (e.g., Bouwens et al. 2004c; Bouwens & Illingworth 2006; Mannucci et al. 2007; Stanway et al. 2008), providing us with additional leverage to constrain the shape of the  $UV$  LF at  $z \gtrsim 7$ . The ultra deep ACS data over the NICMOS parallels to the HUDF will also allow us to increase both the depth and robustness of our searches

for  $z \sim 8 - 10$  galaxies.

We will organize this paper as follows. In §2, we will provide a brief description of the observations we will use in this paper. In §3, we will describe how we select our dropout samples from the imaging data and how we estimate the likely contamination levels. In §4, we will use these samples to derive the rest-frame  $UV$  LF at  $z \sim 7$  and set constraints on this LF at  $z \sim 9$ . Finally, in §5, we discuss our results, and in §6 we will provide a summary of the main conclusions from this work and provide a short outlook for future progress. Throughout this work, we will find it convenient to denote luminosities in terms of the characteristic luminosity  $L_{z=3}^*$  at  $z \sim 3$  (Steidel et al. 1999), i.e.,  $M_{UV,AB} = -21.07$ . Where necessary, we assume  $\Omega_0 = 0.3$ ,  $\Omega_\Lambda = 0.7$ ,  $H_0 = 70$  km/s/Mpc. Although these parameters are slightly different from those determined from the WMAP five-year results (Dunkley et al. 2008), they allow for convenient comparison with other recent results expressed in a similar manner. Our  $z$  and  $J$  dropout criteria select galaxies over a range in redshift (i.e.,  $z \sim 6.5 - 8.0$  and  $z \sim 8 - 10$ , respectively), with mean redshifts  $\langle z \rangle = 7.3$  and  $\langle z \rangle = 9.0$ , respectively (see §4.2). For succinctness, we will usually refer to the redshift ranges selected by these dropout criteria as  $z \sim 7$  and  $z \sim 9$ . We will express all magnitudes in the AB system (Oke & Gunn 1983).

## 2. OBSERVATIONAL DATA

A summary of the observational data used to search for  $z \gtrsim 7$   $z$  and  $J$  dropouts is provided in Table 1.

### 2.1. NICMOS Search Fields with Deep $zJH$ coverage

Our deepest, wide-area constraint on the rest-frame  $UV$  LF at  $z \sim 7 - 10$  comes from the numerous HST NICMOS NIC3 fields which lie in and around the two GOODS fields. Our reductions of the NICMOS data over and around the GOODS fields (including the HUDF NICMOS data) was performed with the python package “micred.py” (Magee et al. 2007) and represent a slight update to the reductions we performed for the Bouwens & Illingworth (2006) work. The most important change in our reduction procedure is that we now include a correction for the non-linear response of the NIC3 camera (de Jong et al. 2006). This has the effect of brightening the measured magnitudes in the  $J_{110}$  and  $H_{160}$  bands by  $\sim 0.15$  and  $\sim 0.05$  mag (relative to what these magnitudes would be without the corrections). Our reductions of the optical ACS data are the same as those considered in our most recent work on the  $UV$  LF at  $z \sim 4 - 6$  (Bouwens et al. 2007) and include essentially all primary and parallel ACS data taken in the vicinity of the two GOODS fields (e.g., Giavalisco et al. 2004a; Bouwens et al. 2004a; Riess et al. 2007; Oesch et al. 2007).

Our primary NICMOS data set includes a somewhat larger number of search fields, some of significant depth, and better optical coverage than was used in our previous search for  $z \sim 7$  galaxies (Bouwens & Illingworth 2006; see Figure 1 from the Supplementary Information). The most notable additions are (1) one ultra deep (28.1 AB mag at  $5\sigma$ )  $\sim 0.7$  arcmin<sup>2</sup> NIC3 pointing within the area of the HUDF (Oesch et al. 2007), (2) ultra deep (28.7 AB mag at  $5\sigma$ ) optical ACS coverage over the second NICMOS parallel to the HUDF (Oesch et al. 2007), and (3)  $\sim 4$  arcmin<sup>2</sup> of additional deep (26.7 AB mag at

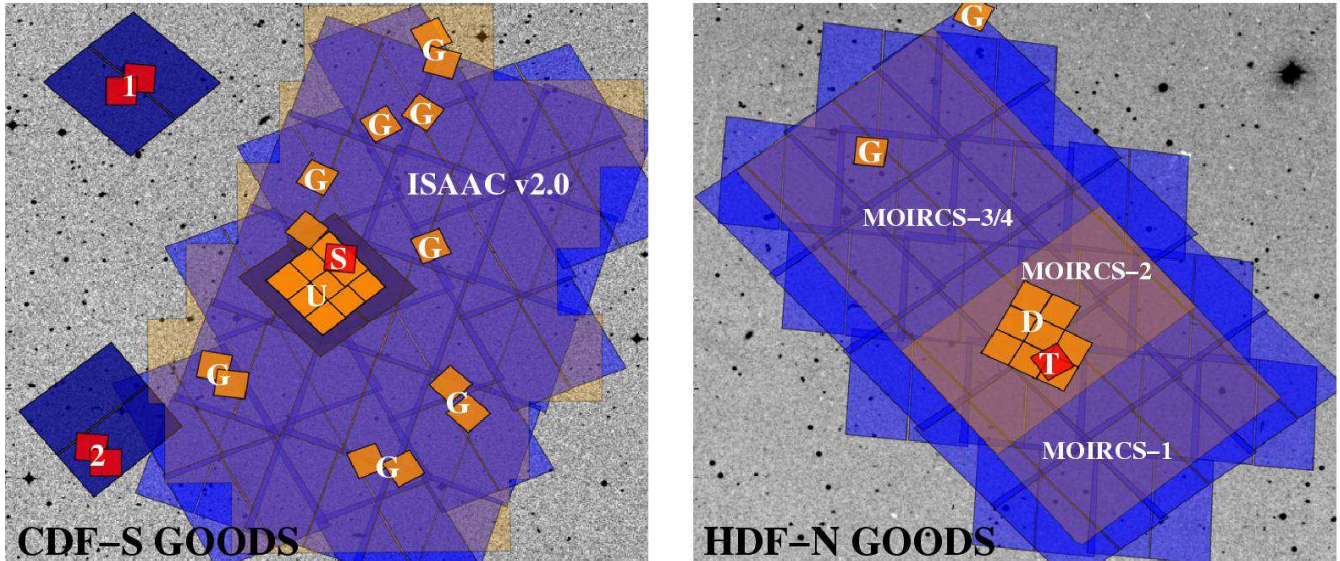


FIG. 1.— Deep near-IR fields in and around the CDF-South (*left*) and HDF-N (*right*) GOODS fields where we conducted searches for star-forming galaxies at  $z \gtrsim 7$  using  $z$  and  $J$  dropout criteria. Areas with deep ( $\gtrsim 28$  mag at  $5\sigma$ ) or ultra-deep ( $\gtrsim 29$  mag at  $5\sigma$ ) optical  $V_{606i775z850}$  coverage are shown in blue and dark blue, respectively. Areas with deep ( $\gtrsim 26.5$  mag at  $5\sigma$ ) or ultra-deep ( $\gtrsim 28$  mag at  $5\sigma$ ) NICMOS coverage are shown in orange and red, respectively. For clarity, we have labelled each of these search fields with a letter, “U” indicating the HUDF Thompson field (Thompson et al. 2005), “S” indicating the HUDF Stiavelli field (Oesch et al. 2007), “D” indicating the HDF-North Dickinson field (Dickinson 1999), “T” indicating the HDF-North Thompson field, (Thompson et al. 1999), “1” indicating HUDF-NICPAR1 (Bouwens et al. 2005; Oesch et al. 2007), “2” indicating HUDF-NICPAR2 (Bouwens et al. 2005; Oesch et al. 2007), and “G” representing the GOODS parallel fields (S. Malhotra et al. 2008, in prep; H. Teplitz et al. 2008, in prep). The deep, wide-area VLT ISAAC coverage of the CDF-South GOODS field is shown as a light orange region. The  $\sim 112$  arcmin<sup>2</sup> of deep MOIRCS coverage (the 4 GTO pointings) over the HDF-North GOODS field is shown with a similar orange shading (the deepest MOIRCS pointing having the darkest shading). Additional information on our search fields can be found in Table 1.

$5\sigma$ ) NICMOS data within the GOODS area (Riess et al. 2007; H. Teplitz et al. 2008, in preparation).

We have also made improvements to our reductions of the two deep NICMOS fields taken in parallel to the HUDF (Bouwens & Illingworth 2006; Oesch et al. 2007: see Figure 1). Reducing the NICMOS data over these fields is challenging because of the small number of unique dither positions used in the acquisition of the data and the large number of individual frames ( $\sim 200$  frames in each field). As a result, any systematics present in characterizing the properties of individual pixels on the NIC3 detector propagate directly into the reduced frames, and therefore it becomes necessary to calibrate these properties sufficiently well so that systematics do not have a dramatic effect on the overall noise characteristics. To accomplish this, we generated super median images from a stack of all the NIC3 frames taken over a field, subtracted this median image from each NIC3 frame, and then redrizzled the individual frames together to produce a cleaner reduction. Before generating the super median images, we mask out all sources identified in the  $\chi^2$  image (Szalay et al. 1999) created from our initial reductions of the  $J_{110}$  and  $H_{160}$  band imaging data;  $\sim 300 - 400$  sources were masked per NIC3 frame. We elected to use the  $\chi^2$  image for this process to ensure that the same sources were masked in both the  $J_{110}$  and  $H_{160}$  frames. Therefore, the colors of sources were not affected by this “median stacking and subtraction” procedure. To obtain the best possible reduction of the data, we repeated the above procedure several times: using each successive reduction of the data to better mask out the faint sources in the data, median stacking the masked frames, subtracting the medians from the individual frames, and then drizzling the data together to

generate a cleaner “final” reduction.

In the dropout searches we performed over the NICMOS data, we only included data which satisfied certain minimal depth requirements in both the optical and near-IR data to avoid the edges of the individual reductions where the number of individual frames contributing to any given pixel was small (i.e., where there might be concerns about some non-Gaussian characteristics in the noise). In our  $z \sim 7$   $z_{850}$ -dropout search, we only included areas where the  $z_{850}$ ,  $J_{110}$ , and  $H_{160}$  depths were 27.5 AB mag, 26.8 AB mag, and 26.5 AB mag, respectively, over a  $0.6''$ -diameter aperture ( $5\sigma$ ). We demanded greater depth for our  $J_{110}$ -band imaging data than we did for the  $H_{160}$ -band data given the importance of a robust detection in the  $J_{110}$ -band to making the case for an object being at  $z \gtrsim 7$ . For our  $z \sim 9$   $J_{110}$ -dropout search, we only included areas where the  $z_{850}$ ,  $J_{110}$ , and  $H_{160}$ -band depths were 27.5 AB mag, 26.8 AB mag, and 26.8 AB mag, respectively, over a  $0.6''$ -diameter aperture ( $5\sigma$ ). We set more stringent requirements on the  $H_{160}$ -band depths for our  $J_{110}$  dropout search because of the greater need to use the  $H_{160}$ -band data to establish the reality of the sources. In total, the area of our search fields were  $\sim 23$  arcmin<sup>2</sup> for our  $z_{850}$ -dropout selection and  $\sim 21$  arcmin<sup>2</sup> for our  $J_{110}$ -dropout selection.

## 2.2. ISAAC Search Fields

The deep ( $J \sim 25.5$  AB mag,  $H, K \sim 25.0$  AB mag at  $5\sigma$ ), wide-area ( $\sim 143$  arcmin<sup>2</sup>) ISAAC data over the CDF-South GOODS field (B. Vandame et al. 2008, in prep; J. Retzlaff et al. 2008, in prep) offer us a superb opportunity to constrain the volume density of very bright star-forming galaxies at  $z \sim 7 - 10$ . While these data are  $\gtrsim 1$  mag shallower than our NICMOS search data

TABLE 1  
PRIMARY IMAGING DATA USED FOR OUR  $z$  AND  $J$  DROPOUT SEARCHES.<sup>a</sup>

Name	Area	$5\sigma$ Depth <sup>b</sup>					Ref <sup>c</sup>
		$z_{850}$	$J_{110}$	$H_{160}$	$K_s$		
HDF-North Dickinson	4.0	27.6	26.8	26.8	25.4	[1,2]	
HDF-North Thompson	0.8	27.6	27.8	27.9	25.4	[3,2]	
HUDF Thompson	5.8	28.8	27.4	27.2	25.8	[4,5]	
HUDF Stiavelli	0.7	28.8	27.9	27.7	25.8	[5,6]	
HUDF-NICPAR1	1.3	28.4	28.4	28.2	–	[6,7]	
HUDF-NICPAR2	1.3	28.4	28.4	28.2	–	[6,7]	
GOODS Parallels	9.3	27.3	26.9	26.7	$\sim 25^d$	[7]	
ISAAC v2.0	136	27.3	$\sim 25.5^d$	$\sim 25.0^d$	$\sim 25^d$	[8,9,10]	
MOIRCS GTO-2	28	27.3	25.4	–	25.4	[2]	
MOIRCS GTO-1,3,4	84	27.3	24.0	–	24.2	[2]	

<sup>a</sup>The layout of these search fields is illustrated in Figure 1.

<sup>b</sup> $5\sigma$  depths for ACS and NICMOS data given in terms of a  $0.6''$ -diameter aperture and in terms of a  $\sim 1.0''$ -diameter aperture for the ground-based  $K_s$ -band data. In contrast to the detection limits quoted in some of our previous work, here our detection limits have been corrected for the nominal light outside these apertures (assuming a point source). The detection limits without this correction are typically  $\sim 0.2$  mag fainter.

<sup>c</sup>References: [1] Dickinson 1999, [2] Kajisawa et al. 2006, Ouchi et al. 2007, [3] Thompson et al. 1999, [4] Thompson et al. (2005), [5] Labbé et al. (2006), [6] Oesch et al. 2007, [7] Bouwens & Illingworth (2006), Riess et al. (2007), H. Teplitz et al. (2008, in prep) [8] B. Vandame et al. 2008, in prep; J. Retzlaff et al. 2007, in prep, [9] Mannucci et al. 2007, and [10] Stanway et al. (2008).

<sup>d</sup>The depth of the near-IR data over the CDF-South varies by  $\sim 0.2 - 0.4$  mag depending upon the observational conditions in which the ISAAC data were taken.

considered above (§2.1), they cover  $\gtrsim 5$  times more area and thus are useful for constraining the volume density of the rarer, more luminous  $UV$ -bright galaxies at  $z \gtrsim 7$ . These data are most useful for searching for  $z_{850}$ -band dropouts due to the greater depth of the ISAAC  $J$ -band data. While Mannucci et al. (2007) used an earlier reduction of these data (v1.5) to search for bright  $z$  dropouts over the CDF-South GOODS field (see also Stanway et al. 2008), here we repeat this selection with our procedures. In doing so, we will be (1) able to more naturally include the search results over these fields with those obtained from our NICMOS fields and (2) be able to take advantage of the additional ISAAC data that have become available over the CDF-S since the completion of the Mannucci et al. (2007) work. The larger data set covers  $\sim 10\%$  more area in the  $J$  and  $K_s$  bands and  $30\%$  more area in the  $H$  band. We will not be using these images to constrain the volume density of  $z \sim 9$   $J$ -dropouts because of the limited depth ( $\sim 25$  mag at  $5\sigma$ ) of the ISAAC  $H$  and  $K_s$  band data.

We make use of the final (v2.0) reductions of the ISAAC data (B. Vandame et al. 2008, in prep; J. Retzlaff et al. 2008, in prep) for our searches. These reductions include  $\sim 143$  arcmin<sup>2</sup> of deep  $J$  and  $K_s$  band coverage and  $\sim 131$  arcmin<sup>2</sup> of deep  $H$  band coverage. Of the area with deep  $J$  and  $K_s$  coverage, only  $\sim 136$  arcmin<sup>2</sup> has deep ACS GOODS coverage. This represents  $4\%$  more area than considered in the  $z$ -dropout search by Mannucci et al. (2007) using the v1.5 ISAAC reductions over the CDF-South GOODS field. The FWHM of the PSF varies from  $\sim 0.35''$  to  $\sim 0.7''$ , with a median value of  $\sim 0.51''$ . The depth of the  $J$ -band data is appropriately  $25.5$  AB mag for a  $4\sigma$  detection, while for the  $H$  and  $K_s$  band data, the depth is  $\sim 24.9$  AB mag. Of course, the actual depth varies by several tenths of a magnitude

across the mosaic depending upon the precise exposure time of the ISAAC data and the FWHM of the PSF. As in the previous section, we used the same reductions of the ACS GOODS data as we used in our latest paper on the UV LF at  $z \sim 4, 5$ , and  $6$  (Bouwens et al. 2007).

### 2.3. MOIRCS Search Fields

We can strengthen our constraints on the prevalence of the bright star-forming galaxies at  $z \gtrsim 7$  by taking advantage of the very deep wide-area data taken over the HDF-North GOODS field. While there have been a number of independent attempts to obtain deep near-IR coverage over this field (e.g., the WIRC data over the HDF-North described by Erb et al. 2006), perhaps the best near-IR data set (i.e., deepest, widest area) is from the Subaru MOIRCS imaging observations (Kajisawa et al. 2006; Ouchi et al. 2007). This is due to the significant investment of telescope time ( $\sim 17$  nights) made by the MOIRCS GTO team in obtaining very deep  $J + K_s$  images during March, April, and May of 2006 (additional observations were made in March and April of 2007 but those are not yet public). There are also 2 nights of high quality  $K_s$  band data available from a separate GO proposal. One of the main science goals for these observations has been to search for  $z \gtrsim 7$  galaxies (e.g., Ouchi et al. 2007).

The raw images were downloaded from the Subaru-Mitaka-Okayama-Kiso Archive (SMOKA: Baba et al. 2002) and then divided into a number of discrete segments, each segment containing  $<50$  images taken one after another in a given filter. Images from each segment were reduced and combined into a single image using the iraf routines in MCSRED (I. Tanaka et al. 2008, in prep). These reductions were then aligned against the ACS GOODS data and then stacked together to produce

two very deep near-IR image mosaics in the  $J$  and  $K_s$  bands. These images were flux calibrated by matching sources with those in the KPNO images of the WFPC2 HDF-North (Dickinson 1998) and in overlap regions between adjacent MOIRCS exposures. Since the MOIRCS GTO team took their observations over 4 distinct pointings, the final reductions cover  $\sim 112$  arcmin<sup>2</sup> in total. The final reductions reach a  $5\sigma$  AB magnitude of 25.4 in the  $J$  band and 25.4 AB mag in the  $K_s$  band over the deepest MOIRCS pointing (GTO-2:  $\sim 28$  arcmin<sup>2</sup>), while the other three pointings (GTO-1,2,4) are some  $\sim 1.3$  mag shallower. The FWHM of the PSF in our reductions was  $\sim 0.5''$  in the  $K_s$  band and  $\sim 0.6''$  in the  $J$  band. The final  $J$ -band image mosaic include some  $\sim 56$  hours of data, and the final  $K_s$  band image mosaic includes some  $\sim 64$  hours of Subaru data.

### 3. SAMPLE CONSTRUCTION

#### 3.1. Catalog Construction

Our procedures for generating PSF-matched catalogues and selecting  $z$  and  $J$ -dropouts are already well-documented in several previous works (e.g., Bouwens et al. 2003; Bouwens et al. 2005; Bouwens & Illingworth 2006; Bouwens et al. 2007). Nonetheless, we will briefly summarize the different steps in our processing here. All images were first PSF-matched to the NICMOS  $H_{160}$ -band data (or  $J$ -band data in the case of our dropout searches over the ISAAC or MOIRCS data). We then ran SExtractor (Bertin & Arnouts 1996) in double-image mode to perform the object detection and photometry. We generated the detection image by taking the square root of  $\chi^2$  image (Szalay et al. 1999) constructed from the  $J_{110}$  and  $H_{160}$  band images for our  $z$ -dropout selection and from the  $H_{160}$  band image for our  $J$ -dropout selection. Colors were measured in a small-scalable aperture using Kron-style (1980) photometry, where the Kron factor was 1.2. These fluxes were then corrected up to total magnitudes using the light within a larger Kron (1980) aperture (adopting a Kron factor of 2.5). These latter corrections were made from the square root of the  $\chi^2$  image to improve the S/N. Figure 5 of Coe et al. (2006) provides a graphical description of a similar multi-stage procedure for measuring colors and total magnitudes. Aperture radii used for total magnitude measurements ranged from  $\sim 0.5$ – $0.8$  arcsec. An additional  $\sim 0.1$ – $0.15$  mag correction was made to account for the light outside of these apertures and on the wings of the PSF (e.g., Thompson et al. 1998).

#### 3.2. Selection Criteria

Our selection criterion for our  $z_{850}$ -dropout search was  $((z_{850} - J_{110})_{AB} > 0.8) \wedge ((z_{850} - J_{110})_{AB} > 0.8 + 0.4(J_{110} - H_{160})_{AB})$  as shown in Figure 2, where  $\wedge$  represents the logical **AND** operation. This criterion is identical to the “less conservative”  $z$ -dropout selection criterion of Bouwens & Illingworth (2006). We opted to use this criterion rather the more stringent “conservative” criterion from that same work for two reasons. First, we realized that our “conservative” criterion may have been more stringent than necessary to reject contaminants like T-dwarfs (low mass stars) from our samples. These contaminants can (in most cases) be rejected by a procedure we will describe below. Second, by adopting a “less conservative” selection criteria, the effective

selection volumes will be larger and therefore less sensitive to small inaccuracies in the assumed model galaxy population.

For regions of the two GOODS fields with ISAAC/MOIRCS coverage, our  $z$ -dropout criterion was  $((z_{850} - J)_{AB} > 1.0) \wedge (J - K_s < 1.2)$ . This selection criterion is very similar to the criterion used over our NICMOS fields. For the typical star-forming galaxy at  $z \sim 7$  (with a  $UV$ -continuum slope  $\beta$  of  $-2$ ) this criterion selects galaxies to a slightly lower-redshift limit  $z \gtrsim 6.5$  than our NICMOS  $z$ -dropout criterion (where  $z \gtrsim 6.6$ ).

The criterion for our  $z \sim 9$   $J_{110}$ -dropout search was  $(J_{110} - H_{160})_{AB} > 1.3$ . We elected to use a less restrictive  $(J_{110} - H_{160})_{AB}$  color criterion than the  $(J_{110} - H_{160})_{AB} > 1.8$  criterion used in our previous  $J$ -dropout search (Bouwens et al. 2005) because of the availability of deep optical data over almost all of our previous search fields to eliminate low redshift interlopers. Previously ultra deep optical data were not available over the NICMOS parallels to the HUDF, and so we accordingly decided to select  $z$  dropouts using a more stringent  $J - H$  color cut.

In computing the  $z - J$  and  $J - H$  colors that we used for our  $z$  and  $J$  dropout selections, we set the  $z$ - and  $J$ -band fluxes to their  $1\sigma$  upper limits in the case of non-detections. This was to minimize the extent to which faint sources in our search fields would scatter into our dropout samples.

Sources in our  $z$  and  $J$ -dropout selections were also required to be detected at the  $4.5\sigma$  level in the  $H_{160}$  band within a  $0.6''$  diameter aperture (to eliminate spurious sources) and undetected ( $< 2\sigma$ ) in the available  $B_{435}$ ,  $V_{606}$ , or  $i_{775}$  band imaging. Sources which were detected at the  $1.5\sigma$  level in more than one of the ACS  $B_{435}$ ,  $V_{606}$ , and  $i_{775}$  bands were also rejected as low-redshift interlopers. Possible contamination by low mass stars (which are a concern for our  $z$ -dropout selection) are identified by looking for sources which showed faint detections ( $> 2\sigma$ ) in the  $z_{850}$ -band in a  $0.2''$ -diameter aperture and whose  $z_{850}$ -band profile appeared to be consistent with a point source (i.e., the SExtractor stellarity parameter  $> 0.6$ ).

All candidate dropouts were inspected in the available IRAC and MIPS coverage over the two GOODS fields (Dickinson & GOODS team 2004) to ensure that none had particularly red  $3.6\mu - 5.8\mu \gtrsim 1$  mag or  $3.6\mu - 24\mu \gtrsim 2$  mag colors. With the exception of the two sources which satisfy our  $J$ -dropout criterion (03:32:41.22,  $-27:44:00.8$  and 03:32:32.45,  $-27:42:21.5$ ), none of the sources which satisfied our other criteria were found to have such red infrared colors (or showed significant detections at  $5.8\mu$ ,  $8.0\mu$ , or  $24\mu$ ).

The two particularly red  $J_{110}$  dropouts (with  $H_{160}$  magnitudes of  $25.7 \pm 0.2$  and  $24.5 \pm 0.1$ , respectively) have  $H_{160} - [4.5\mu]$  colors of  $\sim 2.5$  mag and are even detected at  $24\mu$  in the available MIPS imaging over the GOODS fields (meaning that their apparent magnitudes at  $24\mu\text{m}$  are  $\lesssim 21.5$  mag). Since we do not expect galaxies at  $z \gtrsim 7$  to be so bright at  $24\mu$  and otherwise so highly reddened (but see also discussion in Wiklind et al. 2007), we have excluded these sources as candidate  $z \sim 9$  galaxies.

#### 3.3. Selection Results



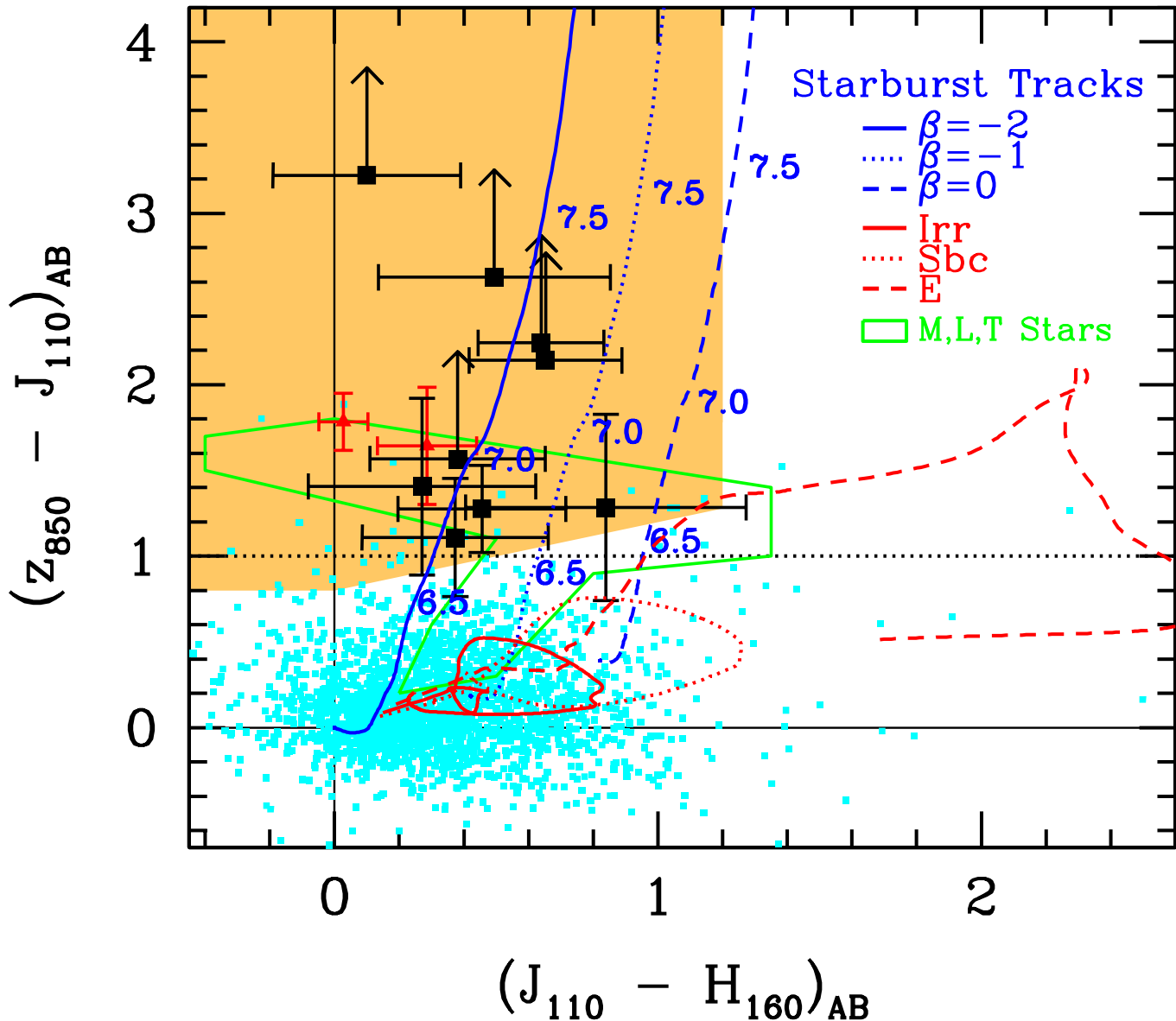


FIG. 2.—  $z - J$  and  $J - H$  color-color diagram illustrating our optical-IR  $z$ -dropout selection window (orange region). The large black squares show the colors of  $z$ -dropouts in our selection (as well as one  $z$ -dropout found behind Abell 1689: Bradley et al. 2008) and their  $1\sigma$  errors (or lower limits). Sources which do not satisfy our  $z$ -dropout selection criteria are shown in cyan. The solid, dotted, and dashed blue lines show how the colors of starbursts with  $UV$ -continuum slopes  $\beta$  of  $-2$ ,  $-1$ , and  $0$ , respectively, vary as a function of redshift. Typical  $UV$ -continuum slopes  $\beta$  observed for star-forming galaxies at  $z \sim 5 - 6$  are  $-2$  (e.g., Stanway et al. 2005; Bouwens et al. 2006; Yan et al. 2005). The red lines show how these colors vary as a function of redshift for low-redshift galaxies (Coleman, Wu, & Weedman 1980). The green lines bracket the region in color-color space where we expect T dwarfs to lie (Knapp et al. 2004). The two red triangles indicate the colors of two bright T dwarfs found in our search (§3.3). While five of the  $z$ -dropout candidates in our selection nominally have  $z - J$  and  $J - H$  colors consistent with that of T-dwarfs, their  $z$ -band flux appears to be extended in all five cases (see also §3.2-§3.4), so these sources cannot be stars.

Application of our selection criteria across all the fields given in Table 1 yielded 8 credible  $z_{850}$ -dropout candidates, but no credible  $J_{110}$ -dropout candidates. All 8 of our  $z$ -dropout candidates were found in our NICMOS search fields. The properties of each of the 8  $z_{850}$ -dropout candidates are given in Table 2. Figure 3 provides a postage stamp montage of the 8 candidates. We also included one candidate we identified in a separate search around massive lensing clusters (Bradley et al. 2008; Bouwens et al. 2008). Five of the eight candidates were given in our two previously published  $z_{850}$ -dropout searches (Bouwens et al. 2004c; Bouwens & Illingworth 2006). Three of these candidates are new. Two of the

three new candidates (UDF-3244-4727 and NICPAR1-3303-4111) were just below the flux thresholds used in our previous searches, but meet these thresholds now as a result of modest improvements in the S/N and overall quality of our NICMOS reductions. The third candidate (NICPAR2-3308-5229) was found over the second NICMOS parallel to the HUDF and could be identified as a result of the much deeper optical (ACS) data now available over these fields to set strong constraints on the  $z - J$  colors. Our sample also includes one  $z_{850}$ -dropout (UDF-380-1125) which, while appearing in the our initial  $z$ -dropout selection over the HUDF (Bouwens et al. 2004c), did not appear in our more recent Bouwens &

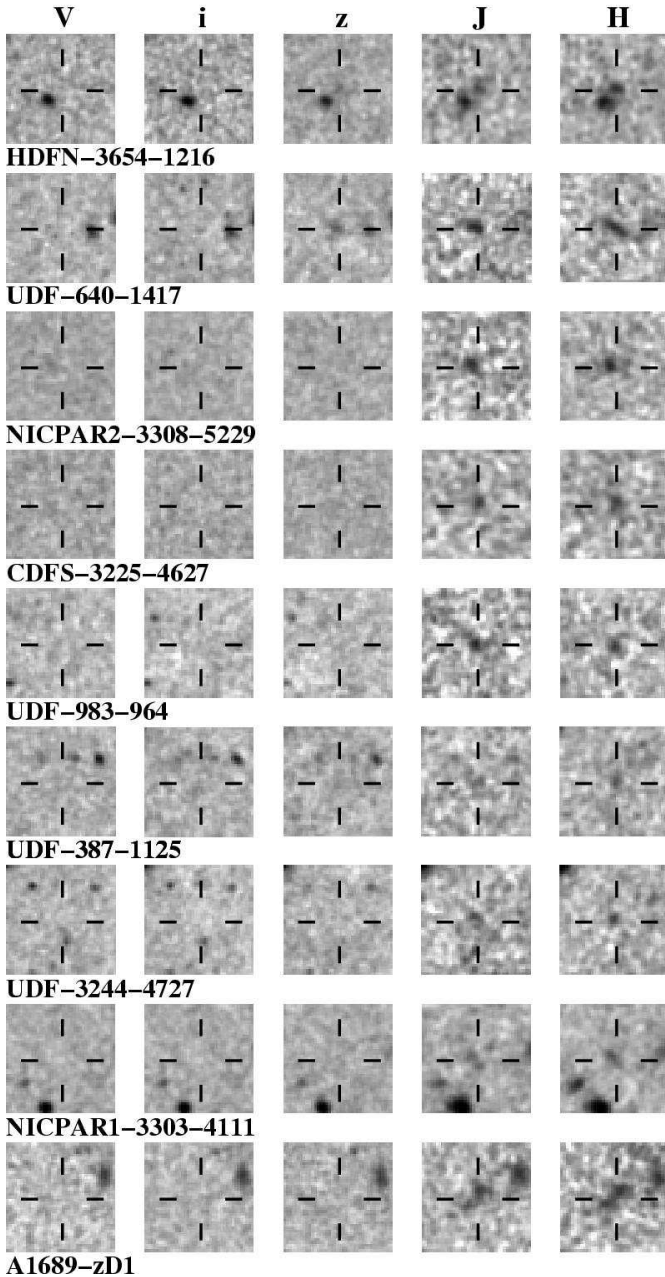


FIG. 3.—  $V_{606}$ ,  $i_{775}$ ,  $z_{850}$ ,  $J_{110}$ , and  $H_{160}$  band cutouts for all eight sources in our  $z \sim 7$   $z_{850}$ -dropout sample. The source presented in the bottom row is another very strong  $z \sim 7$   $z$ -dropout candidate found in an independent search around massive lensing clusters (Bradley et al. 2008; Bouwens et al. 2008). All the sources in our sample are detected at  $> 4.5\sigma$  in both the  $J_{110}$  and  $H_{160}$  bands, with the exception of UDF-3244-4727 and UDF-387-1125 which is only detected at  $3\sigma$  in the  $J_{110}$  band (we will be obtaining deeper  $J_{110}$ -band imaging data for these latter two sources as part of an approved HST program). All the sources in our sample show strong  $z - J$  breaks and are completely undetected ( $< 2\sigma$ ) in the  $V_{606}$  and  $i_{775}$  bands (see §3.2).

Illingworth (2006) selection because of the more conservative S/N threshold used in that work.

There were two sources in our catalogues which while satisfying our  $z$ -dropout color criteria did not make it into our  $z$ -dropout selection because of their compactness in the  $z$ -band, which strongly suggested they were T dwarfs (03:32:25.10,  $-27:46:35.6$  and 12:37:34.26, 62:18:31.4). These sources had previously been identified as possible T dwarfs in a number of other stud-

ies (Bouwens & Illingworth 2006; Mannucci et al. 2007; Eyles et al. 2007). There were also 28 sources in our selection that while satisfying our  $z$ -dropout color criteria showed significant detections ( $> 2\sigma$ ) in the  $B_{435}$ ,  $V_{606}$ , or  $i_{775}$  bands and thus were excluded from our  $z$ -dropout selection. One possible  $z$ -dropout candidate over the near-IR ISAAC data was found at 03:32:24.74,  $-27:55:15.8$ . This source seemed to be a plausible  $z \sim 7$  candidate, with an apparent  $5\sigma$  detection in the  $J$  band, an apparent  $J$ -band magnitude of  $24.8 \pm 0.2$  AB mag, and no detection ( $< 1\sigma$ ) in any of the optical imaging data. However, since this source is undetected ( $H_{AB} > 26.0$  [ $3\sigma$  limit] in a  $1''$ -diameter aperture) in even deeper NICMOS  $H_{160}$ -band data over this field, it seems highly likely that this source is spurious (or perhaps a SNe: see §3.4).

In Appendix D, we discuss several sources which appeared in previous  $z \gtrsim 7$  dropout samples of ours but do not appear in the current selections.

### 3.4. Contamination

We give particular attention to contamination, since it can be a significant issue in searches for very faint, high-redshift galaxies. This discussion is only relevant for our  $z_{850}$ -dropout selection since our  $J_{110}$ -dropout selection contains no credible candidates. There are four types of contaminants that are of particular concern: (i) T-dwarfs, (ii) supernovae, (iii) lower-redshift galaxies which may move into our  $z_{850}$ -dropout selection through photometric scatter, and (iv) spurious sources.

*Possible Contamination from T dwarfs:* T dwarfs are low-mass brown dwarfs, which while most well known and studied in the solar neighborhood (e.g., Knapp et al. 2004; Burgasser et al. 2006), are sometimes observed at great distances and therefore can be quite faint (i.e.,  $J_{AB} \sim 26$ : Ryan et al. 2005; Bouwens & Illingworth 2006). Since T dwarfs occupy a position in color-color space very similar to that of high-redshift galaxies (Figure 2), they can therefore be difficult to distinguish from star-forming galaxies at  $z \sim 7$  on the basis their photometry alone. This leaves us with the size or morphology of these sources as essentially our only means of distinguishing these sources from  $z \sim 7$  galaxies. This enterprise is made more difficult because the T dwarfs are brightest in exactly the same data (near-IR) where the resolution is the poorest. Fortunately, the available ACS data have sufficient depth and resolution that any T dwarfs in our data should show up as  $\gtrsim 5\sigma$  point sources. This follows from the fact that all candidate dropouts in our sample are detected at  $\gtrsim 4.5\sigma$ ; T dwarfs have  $z - J$  colors of  $\sim 1 - 2$  mag, and the ACS  $z_{850}$ -band data are at least  $\sim 2$  mag deeper in a  $0.2''$ -diameter aperture (ACS resolution) than our near-IR data is in a  $0.6''$ -diameter aperture (near-IR resolution: see Table 1).<sup>1</sup> Since none of the  $z$ -dropouts in our selection show  $\gtrsim 4\sigma$ -pointlike detections in the available  $z_{850}$ -band coverage, this suggests that these sources are not T dwarfs.

*Possible Contamination from Supernovae:* Since the NICMOS  $JH$  data were largely taken at quite different times than the ACS  $BViZ$  data, it is quite possible that highly time-variable sources like supernovae could show

<sup>1</sup> The  $5\sigma$  depths of the ACS data in a  $0.2''$ -diameter aperture is  $\sim 1.2$  mag deeper than that given in Table 1 (for a  $0.6''$ -diameter aperture).

TABLE 2  
 $z_{850}$ -DROPOUT CANDIDATES.

Object ID	R.A.	Dec	$H_{160}$	$z_{850} - J_{110}$	$J_{110} - H_{160}$	$H_{160} - K_s$	Ref <sup>a</sup>
HDFN-3654-1216	12:36:54.12	62:12:16.2	$26.0 \pm 0.1$	$1.1 \pm 0.3$	$0.4 \pm 0.3$	$0.0 \pm 0.3$	[2]
UDF-640-1417	03:32:42.56	-27:46:56.6	$26.2 \pm 0.1$	$1.3 \pm 0.3$	$0.5 \pm 0.2$	$0.5 \pm 0.3$	[1,2,3,4,5]
NICPAR2-3308-5229 <sup>b</sup>	03:33:08.29	-27:52:29.2	$26.7 \pm 0.1$	$> 2.2^c$	$0.6 \pm 0.2$	—	—
CDFS-3225-4627	03:32:25.22	-27:46:26.7	$26.7 \pm 0.2$	$1.4 \pm 0.5$	$0.2 \pm 0.3$	$< 0.2^c$	[2]
UDF-983-964	03:32:38.80	-27:47:07.2	$26.9 \pm 0.2$	$> 3.2^c$	$0.1 \pm 0.3$	$0.0 \pm 0.8$	[1,2,4,5]
UDF-387-1125	03:32:42.56	-27:47:31.4	$27.1 \pm 0.2$	$1.3 \pm 0.5$	$0.8 \pm 0.4$	$< 0.0^c$	[1,5]
UDF-3244-4727	03:32:44.02	-27:47:27.3	$27.3 \pm 0.2$	$> 2.6^c$	$0.5 \pm 0.4$	$< 0.1^c$	—
NICPAR1-3303-4111 <sup>d</sup>	03:33:03.81	-27:41:12.1	$27.8 \pm 0.1$	$> 1.5^c$	$0.4 \pm 0.2$	—	—
A1689-zD1 <sup>e</sup>	13:11:29.73	-01:19:20.9	$24.7 \pm 0.1$	$> 2.2^c$	$0.6 \pm 0.2$	—	[6]

<sup>a</sup>References: [1] Bouwens et al. (2004c), [2] Bouwens & Illingworth (2006), [3] Yan & Windhorst (2004), [4] Coe et al. (2006), [5] Labbé et al. (2006), [6] Bradley et al. (2008)

<sup>b</sup>There appears to be some flux in the  $V_{606}$  band very close to the position of this source ( $\sim 0.1''$ ). If this flux is associated with this source and not a chance superposition, it would rule out this source being a  $z \gtrsim 7$  galaxy. The existence of a small amount of flux in the  $V_{606}$  band would be somewhat unexpected given that there is no detectable flux in the  $i_{775}$  and  $z_{850}$  bands and the fact that these exposures reach similar flux limits. On balance, we consider this to be a likely  $z \sim 7$  candidate.

<sup>c</sup>Upper and lower limits on the measured colors are the  $1\sigma$  limits.

<sup>d</sup>Because this source (detected at  $\sim 5-6\sigma$ ) was found over the NICMOS parallels to the HUDF and the noise properties of these data may exhibit significant non-Gaussian characteristics due to the small number of unique dither positions (see §2.1), we took special care in assessing the reality of this source. We considered all the available NICMOS data at 4 highly distinct dither positions (separated by  $\sim 2-3''$  each) and in both the  $J_{110}$  and  $H_{160}$ -band data separately. The candidate was evident at  $\gtrsim 2-3\sigma$  significance in 7 of the 8 of the stacks, consistent with what we might expect if the candidate were a real source. This source is also present in an independent reduction of these data (Oesch et al. 2008).

<sup>e</sup>This source was identified in a separate search for  $z \sim 7$   $z$ -dropouts behind massive galaxy clusters (Bradley et al. 2008; Bouwens et al. 2008) and is not used here for deriving the UV LF at  $z \sim 7$ . This source is substantially magnified by gravitational lensing from Abell 1689 ( $\mu \sim 9.3$ ). Its delensed  $H_{160}$ -band magnitude is  $\sim 27.1$  AB mag (Bradley et al. 2008).

up as dropouts in our selections. To estimate the approximate frequency at which we might expect such sources to show up in our searches, we adopted the GOODS supernova searches (Riess et al. 2004; Strolger et al. 2004) as a baseline. In their searches, they identified 42 supernovae in 8 independent searches over one of the two  $\sim 160$  arcmin<sup>2</sup> GOODS fields (15 ACS WFC pointings), or  $\sim 1/3$  supernovae per  $\sim 11$  arcmin<sup>2</sup> ACS WFC field per  $\sim 40$  day period. Of these supernovae, only  $\sim 40\%$  of the high-redshift supernovae identified by Riess et al. (2004) and Strolger et al. (2004) appear to be well enough separated from their host galaxies to be identified as a separate source. Having calculated the approximate rate at which supernovae appear at random in deep fields, all that remains is to calculate the time period over which we might expect these supernovae to show up as possible sources in our search. While theoretically we might expect high-redshift SNe to be bright enough to show up in our survey data for  $\sim 100$  days (if we take the typical light curves found in e.g., Strolger et al. 2004), all  $z$ -dropouts in our sample are within  $\sim 1$  mag of the flux limit of each survey field. Typical SNe (at  $z \sim 1$ ) would not remain at these magnitudes for more than  $\sim 40$  days, so the incidence of SNe in our probe should be  $\sim (1/3)(1/11\text{arcmin}^2)(0.40) \sim 0.012$  arcmin<sup>-2</sup> for data taken at different epochs. Multiplying this by the  $\sim 16$  arcmin<sup>2</sup> of NICMOS data in our search taken at significantly different times than the ACS data (the HUDF NICMOS data were taken at a similar time to the ACS HUDF data), we would expect that only  $\sim 0.2$  supernovae should contaminate our high redshift selections. While this number is just 3% of the 8 sources in our  $z$ -dropout selection and therefore likely of minimal importance for

the present LF determinations, it does indicate that contamination of high-redshift selections by supernovae is a real possibility. This may be a particularly important concern in searches for bright  $z \gtrsim 7$  galaxies due to the inherent rarity of those sources.

*Possible Contamination Through Photometric Scatter:* One possible source of contamination are low redshift sources scattering into our color selection simply because of noise. To assess the importance of this effect, we ran a number of Monte-Carlo simulations where we started with a low-redshift galaxy population and then added noise to the fluxes in the individual bands to see how many of the sources would satisfy our  $z_{850}$ -dropout selection. Clearly, the most critical aspect of these simulations is ensuring that the properties of the input galaxy population (to which noise is added) are accurate. We set up the input population as follows: (1) The input  $H_{160,AB}$  magnitudes and photometric errors are modelled using the actual distribution of magnitudes and errors found in the data (to make our estimates as model independent as possible and because essentially all faint sources in our fields will be at  $z < 6.5$ ) and (2) The colors (i.e., optical- $H_{160}$  and  $J_{110} - H_{160}$ ) of the input population are assumed to be distributed in the same way as is observed for galaxies in the range  $24.5 < H_{160,AB} < 26$  in the HUDF (ACS+NICMOS coverage). We used galaxies in this magnitude range because of their higher S/N colors and because the multivariate color distribution is similar (albeit slightly redder) to galaxies at  $H_{160}$ -band magnitudes  $\gtrsim 26$  AB mag. This magnitude range also does not include any sources which are candidate  $z \sim 7$  galaxies (at least in the HUDF).

Based upon the described input population, we ran



10 separate photometric scattering experiments for each search field. We estimated that there would be 0.0, 0.3, 0.2, and 0.3 low-redshift contaminants, respectively, for our  $z$ -dropout selections over the HUDF, NICPAR, HDFN, and GOODS parallel fields. In total,  $\sim 0.8$  contaminants are expected from all our fields. We note that the approach taken here to estimate contamination from photometric scatter is analogous to the one described in Bouwens et al. (2004c) or Appendix D.4.2 of Bouwens et al. (2006).

*Possible Contamination from Spurious Sources:* Finally, to estimate the number of contaminants from spurious sources, we repeated our selection procedure on the negative images (e.g., Dickinson et al. 2004; Yan & Windhorst 2004; Bouwens et al. 2007) and found no sources that satisfied our selection. This suggests that the spurious fraction is negligible. We note that we would not expect contamination from spurious sources to be a problem since essentially all of the sources in our sample are detected at  $\geq 4.5\sigma$  in both the  $J_{110}$  and  $H_{160}$  bands. The only notable exceptions to this are for the two sources in our sample, UDF-387-1125 and UDF-3244-4727, where  $J_{110}$ -band detections are still only at the  $3\sigma$  level. However, in both cases, we are attempting to improve the detection significance (as well as the S/N of the  $z - J$  and  $J - H$  colors) by obtaining an additional 9-12 orbits of  $J_{110}$ -band data on both sources (likely improving their detection significance to the  $4.5\sigma$  level).

In summary, the overall level of contamination should be fairly low in general. We would expect  $\sim 0.8$  galaxy to enter our sample from photometric scatter,  $\sim 0.2$  SNe contaminants to enter our sample, and there to be no contamination from T dwarfs or spurious sources. Overall, this suggests an overall contamination level of  $\sim 12\%$ .

#### 4. DETERMINATIONS OF THE UV LF AT $Z \sim 7 - 10$

We now utilize our search results to determine the rest-frame  $UV$  LF at  $z \sim 7$ . We will consider both LFs using both stepwise and Schechter parametrizations. The advantage of the stepwise determinations is that they give a more model-independent measure of the constraints we have on the LF, while the Schechter determinations are more amenable to direct interpretation and comparison with other determinations in the literature.

As in other methodologies for determining the LF, we maximize the probability with which our model LFs are able to reproduce our search results. Since we do not know the precise redshifts for our sources, our goal will simply be to reproduce the surface density of  $z$ -dropout candidates in each of our search fields as a function of apparent magnitude. This is similar to the modelling we performed in our previous paper on the  $UV$  LFs at  $z \sim 4$ ,  $z \sim 5$ , and  $z \sim 6$  (Bouwens et al. 2007), where we attempted to reproduce the surface density of  $B$ ,  $V$ , and  $i$  dropouts in deep ACS fields.

To maximize the likelihood with which our model LFs reproduce our search results, we need to be able to compute the expected surface density of dropouts as a function of magnitude. We use a similar formalism to the one we used in our previous paper on the LFs at  $z \sim 4 - 6$ :

$$\Sigma_k \phi_k V_{m,k} = N_m \quad (1)$$

where  $N_m$  is the surface density of galaxies in some search field with magnitude  $m$ ,  $\phi_k$  is the volume density of

galaxies with absolute magnitude  $k$ , and  $V_{m,k}$  is the effective selection volume for which galaxies with absolute magnitude  $k$  will both satisfy our dropout selection criteria and be observed to have an apparent magnitude  $m$ . The width of the magnitude bins in  $N_m$ ,  $\phi_k$ , and  $V_{m,k}$  will depend upon the LF parameterization we consider (stepwise vs. Schechter).

We computed the effective volumes  $V_{m,k}$  for our  $z$  and  $J$  dropout selections by artificially redshifting  $B$ -dropouts from the HUDF across the selection windows of our higher redshift samples, adding the sources to the real data, and then repeating our selection procedure. We used our well-tested cloning software (Bouwens et al. 1998a,b; Bouwens et al. 2003) to handle the artificial redshifting of sources from  $z \sim 4$  to  $z \sim 6 - 10$ . The size of the sources were scaled as  $(1+z)^{-1.1}$  (independent of luminosity) to match the size trends observed for star-forming galaxies at  $z \gtrsim 2$  (Bouwens et al. 2006; see also Ferguson et al. 2004 and Bouwens et al. 2004c). The redshifted (“cloned”) sources were smoothed so that their effective PSFs matched that seen in the data. The mean  $UV$ -continuum slope  $\beta$  was set to  $-2$  to agree with that observed in  $L_{z=3}^*$  star-forming galaxies at  $z \sim 6$  (Stanway et al. 2005; Bouwens et al. 2006; Yan et al. 2005) while the  $1\sigma$  dispersion in  $\beta$  was set to 0.5, which is similar to what is found at  $z \sim 4 - 6$  (e.g., Bouwens et al. 2007; R.J. Bouwens et al. 2008, in prep). Instead of using simple power laws to represent model SEDs of given  $UV$  continuum slope  $\beta$ , we elected to use  $10^8$ -yr continuous star-formation models (Bruzual & Charlot 2003) where the dust extinction (Calzetti et al. 1994) is varied to reproduce the model slopes. This should provide for a slightly more realistic representation of the SEDs of star-forming galaxies at  $z \gtrsim 7$  than can be obtained from simple power law spectra.

To evaluate the likelihood with which the surface densities computed above would reproduce that found in the observations, we assumed simple Poissonian statistics and compared the observed and expected numbers bin by bin. In detail, our expression for the likelihood  $\mathcal{L}$  is

$$\mathcal{L} = \prod_{i,j} e^{-N_{exp,i,j}} \frac{(N_{exp,i,j})^{N_{obs,i,j}}}{(N_{obs,i,j})!} \quad (2)$$

where  $N_{obs,i,j}$  is the observed number of sources in search field  $i$  and magnitude interval  $j$ , where  $N_{exp,i,j}$  is the expected number of sources in search field  $i$  and magnitude interval  $j$ , and where  $\prod_{i,j}$  is the product symbol. We elected to use the above procedure instead of a more conventional procedure like STY79 (Sandage, Tammann, & Yahil 1979) or SWML (Efstathiou et al. 1988: which determine the shape of the LF independent of the normalization) to take advantage of our search constraints on the volume density of bright  $z \gtrsim 7$  galaxies from our wide-area ground-based data. Maximum likelihood procedures (like SWML or STY79) do not take advantage of these null search results – simply because there are no sources to use for estimating the shape of the LF. While the maximum likelihood fit results from Eq. 2 will be affected by large-scale structure variations across our search fields, we will compute the uncertainties which result from these variations in §4.1, §4.2, and Appendix A and include them in our overall error budget.

In determining the rest-frame  $UV$  LF at  $z \sim 7$  and

$z \sim 9$  from our  $z$  and  $J$  dropout selections, we will adopt  $z \sim 7.3$  and  $z \sim 9.0$ , respectively, as the fiducial redshifts for these selections and the derived LFs. In §4.2, we will justify the use of these mean redshifts using the effective volume simulations just described (see also Bouwens et al. 2004; Bouwens et al. 2005; Bouwens & Illingworth 2006).

#### 4.1. Stepwise Determinations

We begin with a determination of the LF at  $z \sim 7$  and  $z \sim 9$  in stepwise form. The advantage of stepwise parametrizations is that they allow us to determine the overall prevalence of galaxies in a way that is very model independent and just a simple function of luminosity. The width of the bins in the LF are 0.8 mag and was chosen as a compromise between the need to have a few  $z \sim 7$  galaxies per bin and the desire to retain a reasonable resolution in luminosity for our derived LFs. We use a similar bin size for the stepwise upper limits on our  $z \sim 9$   $J$ -dropout LF in order to make these limits more easily interpretable. The stepwise LF  $\phi_k$  is then derived using Eq. 1. The results are presented in Table 3.

Perhaps the largest uncertainties in these LF determinations arise from small number statistics (Poissonian errors). However, in addition to the simple number statistics, there are also sizeable uncertainties that come from large-scale structure variations as well as our effective volume estimates. Let us first consider the uncertainties coming from large-scale structure variations. Adopting a pencil beam geometry, redshift selection window with width  $\Delta z = 1.5$ , search area of 100 arcmin<sup>2</sup>, and bias of 7 (which is appropriate for sources with volume densities of  $\sim 10^{-3.5}$  Mpc<sup>-3</sup>; e.g., Mo & White 1996; Somerville et al. 2004; Trenti & Stiavelli 2008), we estimate a  $1\sigma$  RMS uncertainty of  $\sim 30\%$  in the  $\phi_k$ 's due to field-to-field variations (see also estimates in Bouwens & Illingworth 2006). At  $z \sim 9$ , these uncertainties are  $\sim 20\%$  assuming a redshift selection window with width  $\Delta z = 2$  (see Bouwens et al. 2005).

Uncertainties in our effective volume estimates derive primarily from our imperfect knowledge of the size (or surface brightness) distribution of star-forming galaxies at  $z \gtrsim 7$ .<sup>2</sup> Fortunately, the mean size of star-forming galaxies at  $z \gtrsim 4$  show a good correlation with redshift (i.e., mean half-light radius  $\propto (1+z)^{-1.1 \pm 0.3}$  for fixed luminosity; Bouwens et al. 2006) and we can make a reasonable estimate for what the size (surface brightness) distribution of galaxies is at  $z \gtrsim 7$ . Nonetheless, this distribution is at least as uncertain as the error on the size-redshift scaling. Propagating the error on this scaling into the size distributions assumed in our effective volume estimates, we estimate an RMS uncertainty of 17% in the selection volume at  $z \sim 7$  and 15% at  $z \sim 9$  due to the uncertainties in the size (surface brightness) distribution. Together the size and large-scale structure uncertainties add an uncertainty of 34% and 25% RMS to each bin of the rest-frame UV LF at  $z \sim 7$  and  $z \sim 9$ , respectively. These uncertainties have been added in quadrature with those deriving from the small number statistics. They are given in Table 3.

<sup>2</sup> Uncertainties in the UV color distribution also contribute to the overall error budget for our effective volume estimates, but they are smaller in general (e.g., see §5.2).

TABLE 3  
STEPWISE CONSTRAINTS ON THE  
REST-FRAME UV LF AT  $z \sim 7$  AND  
 $z \sim 9$  (§4.1).

$M_{UV,AB}$ <sup>b</sup>	$\phi_k$ (Mpc <sup>-3</sup> mag <sup>-1</sup> )
<i>z</i> -dropouts ( $z \sim 7$ )	
-21.55	< 0.000003 <sup>a</sup>
-20.84	0.00005 <sup>+0.00007</sup> <sub>-0.00003</sub>
-20.04	0.00029 <sup>+0.00024</sup> <sub>-0.00014</sub>
-19.24	0.00063 <sup>+0.00085</sup> <sub>-0.00041</sub>
<i>J</i> -dropouts ( $z \sim 9$ )	
-21.95	< 0.000019 <sup>a</sup>
-21.15	< 0.000023 <sup>a</sup>
-20.35	< 0.000082 <sup>a</sup>
-19.55	< 0.000687 <sup>a</sup>

<sup>a</sup>Upper limits here are  $1\sigma$  (68% confidence).

<sup>b</sup>The effective rest-frame wavelength is  $\sim 1900\text{\AA}$  for our  $z$ -dropout selection and  $\sim 1500\text{\AA}$  for our  $J$ -dropout selection.

These LFs are also presented in Figure 4 with the magenta points for our  $z \sim 7$  LF and black downward arrows for the constraints on the  $z \sim 9$  LF. A comparison with previous determinations at  $z \sim 4$ ,  $z \sim 5$ , and  $z \sim 6$  from Bouwens et al. (2007) is also included on this figure for context. Though the error bars for individual points in the LF at  $z \sim 7$  are still quite sizeable, there is strong evidence that the UV LF at  $z \sim 7$  is different from the UV LF at  $z \sim 6$  (99% confidence) and thus there is evolution from  $z \sim 7$  to  $z \sim 6$ . We determined this confidence level by finding the value of  $M^*$  and  $\phi^*$  which minimizes the total  $\chi^2$  evaluated for our  $i$  and  $z$  dropout LFs and then looking at the probability of obtaining the resultant reduced- $\chi^2$  purely by chance. This conclusion was already drawn by Bouwens & Illingworth (2006) on the basis of a smaller but very similar selection of galaxies.

#### 4.2. Schechter Determinations

We will now attempt to express the results of our search for  $z \gtrsim 7$  galaxies using a Schechter parameterization. The Schechter parametrization is convenient since it is much more amenable to interpretation than stepwise LFs are. Of course, it is not at all clear from the stepwise LFs derived in §4.1 (particularly given the sizeable observational uncertainties) that the UV LF at  $z \gtrsim 7$  is well described by a Schechter function (see discussion in §5.5).

As with our stepwise determinations, we will calculate the expected surface density of dropouts given a model LF by using Eq. 1 and expressing the Schechter function in stepwise form. For convenience, we have decided to bin the surface density of galaxies in magnitude intervals of width 0.1 mag. Use of substantially finer bins does not have a noticeable effect on the results. Because of the size of current  $z \sim 7 - 10$  samples and limited luminosities ( $\lesssim -19$  AB mag) to which we can probe, we cannot hope to obtain very strong constraints on the faint-end slope of the LF at  $z \gtrsim 7$  and therefore it makes sense for us to fix it to some fiducial value. We will adopt  $-1.74$ , which is the faint-end slope of the UV LF at  $z \sim 6$  determined by Bouwens et al. (2007) using the HUDF and a large

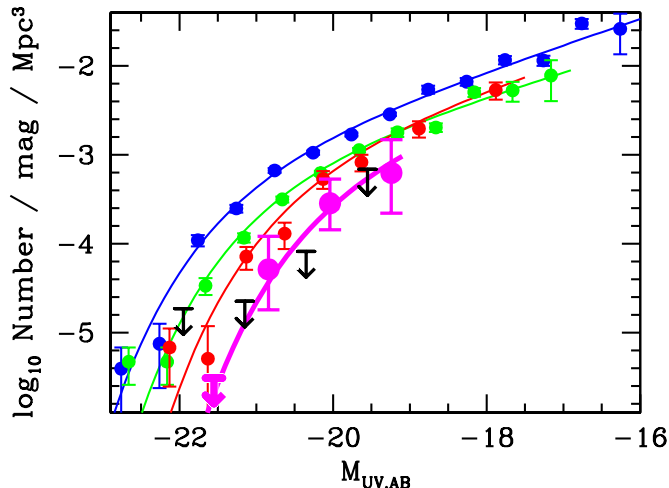


FIG. 4.— Determinations of the rest-frame  $UV$  luminosity function (LF) at  $z \sim 7$  using both a Schechter parameterization (magenta line) and in stepwise form (magenta circles with  $1\sigma$  error bars). Note that the stepwise and Schechter determinations of the LF are determined separately (i.e., our Schechter LF fits are not obtained through fits to our stepwise LFs). The lines are not fits to the points. The  $1\sigma$  upper limits on the bright end of the  $UV$  LF at  $z \sim 7$  and at  $z \sim 9$  are shown with the downward arrows in magenta and black, respectively. For context, we have included the rest-frame  $UV$  LFs determined by B07 at  $z \sim 4$  (red symbols),  $z \sim 5$  (green symbols), and  $z \sim 6$  (red symbols).

TABLE 4  
COMPARISON OF THE SCHECHTER PARAMETERS FOR THE REST-FRAME  $UV$  LFs AT  $z \sim 7$  AND  $z \sim 9$  WITH DETERMINATIONS AT  $z \sim 4$ ,  $z \sim 5$ , AND  $z \sim 6$  FROM BOUWENS ET AL. (2007).

Dropout Sample	$\langle z \rangle$	$M_{UV}^*$ <sup>a</sup>	$\phi^*$ ( $10^{-3}$ Mpc $^{-3}$ )	$\alpha$
$z$	7.3	$-19.8 \pm 0.4$	$1.1^{+1.7}_{-0.7}$	$(-1.74)^b$
$J$	9.0	$> -19.6^c$	$(1.1)^b$	$(-1.74)^b$
$B$	3.8	$-20.98 \pm 0.10$	$1.3 \pm 0.2$	$-1.73 \pm 0.05$
$V$	5.0	$-20.64 \pm 0.13$	$1.0 \pm 0.3$	$-1.66 \pm 0.09$
$i$	5.9	$-20.24 \pm 0.19$	$1.4^{+0.6}_{-0.4}$	$-1.74 \pm 0.16$

<sup>a</sup>Values of  $M_{UV}^*$  are at  $1600 \text{ \AA}$  for the Bouwens et al. (2007)  $B$  and  $V$ -dropout LFs, at  $\sim 1350 \text{ \AA}$  for the Bouwens et al. (2007)  $i$ -dropout LF, at  $\sim 1900 \text{ \AA}$  for our  $z$ -dropout LF, and at  $\sim 1500 \text{ \AA}$  for our constraints on the  $J$ -dropout LF. Since  $z \sim 6$  galaxies are blue ( $\beta \sim -2$ ; Stanway et al. 2005; B06), we expect the value of  $M_{UV}^*$  at  $z \sim 6$  to be very similar ( $\lesssim 0.1$  mag) at  $1600 \text{ \AA}$  to its value at  $1350 \text{ \AA}$ . Similarly, we expect the value of  $M_{UV}^*$  at  $z \sim 7$  and  $z \sim 9$  to be fairly similar at  $\sim 1600 \text{ \AA}$  to the values determined at  $\sim 1900 \text{ \AA}$  and  $\sim 1500 \text{ \AA}$ , respectively.

<sup>b</sup>Fixed in our fits (§4.2)

<sup>c</sup>Lower limits here are  $1\sigma$  (68% confidence).

number of deep ACS fields. Later we will investigate the sensitivity of our results to the value we assume for the faint-end slope.

Our best-fit Schechter parameters at  $z \sim 7$  for our  $z$ -dropout selection are  $M_{AB}^* = -19.8 \pm 0.4$  mag and  $\phi^* = 0.0011^{+0.0017}_{-0.0007}$  Mpc $^{-3}$  for a fixed faint-end slope  $\alpha = -1.74$ . The 68% and 95% likelihood contours for these parameters are given in Figure 5 and compared with our previous determinations from our  $B$ ,  $V$ , and  $i$ -dropout selections at  $z \sim 4$ ,  $z \sim 5$ , and  $z \sim 6$ , respec-

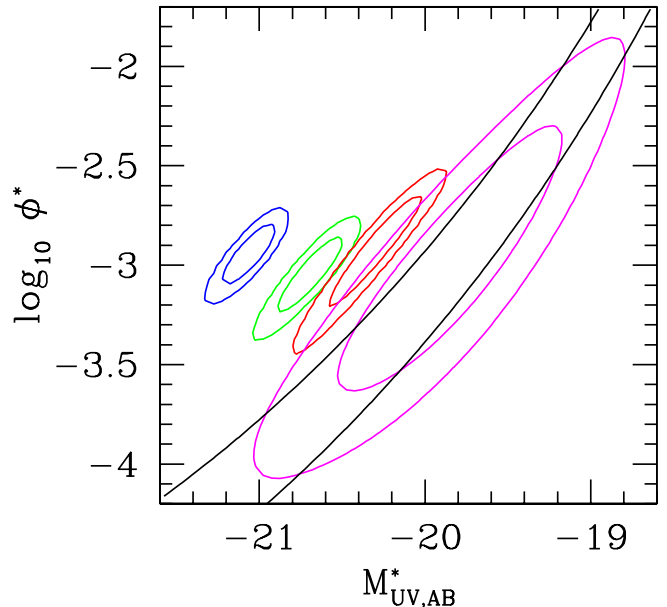


FIG. 5.— 68% and 95% likelihood intervals on the Schechter parameters  $M^*$  and  $\phi^*$  for the rest-frame  $UV$  luminosity function (LF) at  $z \sim 7$  (magenta contours) and  $z \sim 9$  (black contours) derived from our  $z$  and  $J$ -dropout search results, respectively (where the left and right black lines represent the 95% and 68% confidence intervals, respectively, on the  $z \sim 9$  LF). Also shown are the likelihood contours Bouwens et al. (2007) derived for the  $UV$  LF at  $z \sim 4$  (blue contours),  $z \sim 5$  (green contours), and  $z \sim 6$  (red contours). These contours are expressed in terms of the Schechter parameters  $\phi^*$  and  $M^*$ . A faint-end slope  $\alpha$  of  $-1.74$  is assumed for the determinations at  $z \sim 7$  and  $z \sim 9$  (to match that seen at  $z \sim 6$ ; Bouwens et al. 2007), but the exact value assumed for  $\alpha$  makes little difference to the derived contours for  $\phi^*$  and  $M^*$  (see §4.2). Not surprisingly, our constraints on the Schechter parameters at  $z \sim 7$  are considerably worse than at  $z \sim 4 - 6$ , reflecting the substantially smaller size of samples at  $z \gtrsim 7$ . Nonetheless, it seems clear that the  $UV$  LF shows significant and consistent evolution towards brighter values of  $M^*$  with cosmic time (by  $\sim 1.2$  mag from  $z \sim 7$  to  $z \sim 4$ ). There is little evidence for evolution in the volume density  $\phi^*$ . Note that our constraints on the  $z \sim 9$  LF rule out no-evolution from  $z \sim 9$  to  $z \sim 7$  at  $\sim 80\%$  confidence. No evolution from  $z \sim 7$  to  $z \sim 6$  is ruled out at 99% confidence.

tively (Bouwens et al. 2007). The best-fit values are also given in Table 4. Large-scale structure uncertainties resulting from field-to-field variations were estimated using Monte-Carlo simulations (Appendix A) and incorporated into the uncertainties quoted above. While the best-fit value for  $\phi^*$  is very similar to that found at  $z \sim 4$  for the Bouwens et al. (2007)  $B$ -dropout selections, the best-fit value for  $M_{UV}^*$  is  $1.2 \pm 0.4$  mag fainter than the value of  $M_{UV}^*$  ( $= -20.98 \pm 0.07$  mag) found at  $z \sim 4$  by Bouwens et al. (2007) and  $0.4 \pm 0.4$  mag fainter than the value of  $M_{UV}^*$  ( $= -20.24 \pm 0.19$  mag) found at  $z \sim 6$  by Bouwens et al. (2007). This suggests that the brightening we observe in  $M_{UV}^*$  from  $z \sim 6$  to  $z \sim 4$  (Bouwens et al. 2006; Bouwens et al. 2007) is also seen from  $z \sim 7$ . Of course, we must admit that we are somewhat surprised that our best-fit Schechter parameters are in such excellent agreement with an extrapolation of lower redshift trends! It would suggest that our  $z$ -dropout sample may largely be made up of star-forming galaxies at  $z \sim 7$  as we have argued in §3.3 and §3.4 (i.e., the number of low-redshift interlopers is small) and that the effective volumes we have estimated for this sample are reasonably accurate (see also discussion in Appendix B).

Given the small size of current  $z$ -dropout samples, it

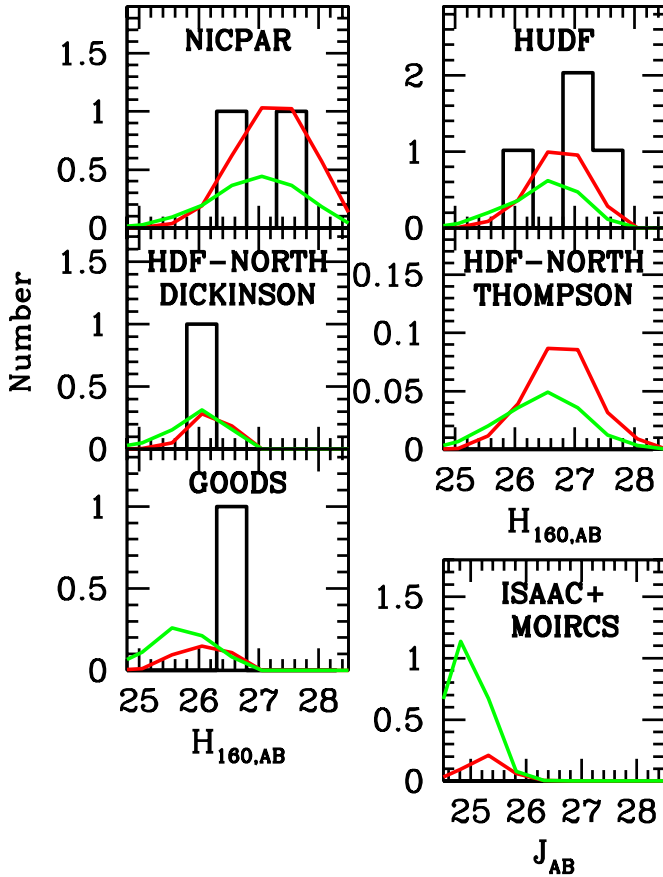


FIG. 6.— Number of  $z$ -dropouts in our search fields (histogram) versus that expected from our best-fit LF (red lines). Panels correspond to searches over the two NICMOS parallels to the HUDF (Bouwens et al. 2005; Oesch et al. 2007), the NICMOS HUDF Thompson & Stiavelli fields (Thompson et al. 2005; Oesch et al. 2007), the HDF-North Dickinson (1999) field, the HDF-North Thompson et al. (1999) field, the CDF-South GOODS ISAAC field (B. Vandame et al. 2008, in prep; J. Retzlaff et al. 2008, in prep; §2.2), the HDF-North GOODS MOIRCS fields (Kajisawa et al. 2006; §2.3) and various NICMOS parallels over the GOODS fields (see Table 1 and Figure 1). Binning is done on 0.5 mag intervals. The green line shows the expected counts if we force our best-fit  $UV$  LF at  $z \sim 7$  to have the same value of  $M_{UV}^*$  and  $\alpha$  as we determined at  $z \sim 4$  and only allow  $\phi^*$  to vary to best fit the data. Clearly, the best-fit LF obtained in this manner (green lines) predicts too many galaxies at bright magnitudes than are observed (e.g.,  $\sim 2-3$  galaxies predicted at  $J_{AB}, H_{160,AB} \sim 25-26$  vs. the 0 observed) and far too few galaxies at fainter magnitudes ( $H_{160,AB} \sim 27-28$ : particularly in the HUDF panel where the observed numbers are  $> 4\times$  larger). This demonstrates that even in the very modest  $z$ -dropout selections which are available there is reasonable ( $\sim 3\sigma$ ) evidence that the typical luminosity of galaxies at  $z \sim 7$  is much fainter than it is at  $z \sim 3-4$ . Of course, despite our ability to draw a few simple conclusions like this, there are still significant uncertainties in deriving the  $UV$  LF from the observed counts.

may seem surprising that we are able to obtain any constraint at all on the shape on the  $UV$  LF at  $z \sim 7$ . Fortunately, the large luminosity range over which we have constraints on the surface density of dropouts (i.e., from 25 AB mag to 28 AB mag) largely makes up for what we lack in statistics. These constraints can be helpful, even brightward of 26.0 AB mag where our  $z$ -dropout sample contains no sources, because of the large search areas we consider ( $\sim 248$  arcmin<sup>2</sup>). To illustrate how our search results help us constrain the overall shape of the  $UV$  LF, we show in Figure 6 the predicted counts for each of our

TABLE 5  
BEST-FIT SCHECHTER PARAMETERS FOR THE  $UV$  LFs AT  $z \sim 7$  AND  $z \sim 9$  WITH DIFFERENT ASSUMED FAINT-END SLOPES.

Dropout Sample	$\langle z \rangle$	$M_{UV}^*$ <sup>a</sup>	$\phi^*$ ( $10^{-3}$ Mpc <sup>-3</sup> )	$\alpha$
$z$	7.3	$-19.8 \pm 0.4$	$1.1^{+1.7}_{-0.7}$	$(-1.74)^b$
$z$	7.3	$-19.6 \pm 0.4$	$1.7^{+2.6}_{-1.1}$	$(-1.4)^b$
$z$	7.3	$-19.9 \pm 0.4$	$0.8^{+1.2}_{-0.5}$	$(-2.0)^b$
$J$	9.0	$> -19.6^c$	$(1.1)^b$	$(-1.74)^b$
$J$	9.0	$> -19.5^c$	$(1.1)^b$	$(-1.4)^b$
$J$	9.0	$> -19.7^c$	$(1.1)^b$	$(-2.0)^b$
$J$	9.0	$(-21.0)^b$	$< 0.06^c$	$(-1.74)^b$
$J$	9.0	$(-21.0)^b$	$< 0.05^c$	$(-1.4)^b$
$J$	9.0	$(-21.0)^b$	$< 0.07^c$	$(-2.0)^b$

<sup>a</sup>See remarks in Table 4.

<sup>b</sup>Fixed in our fits (§4.2)

<sup>c</sup>Lower limits here are  $1\sigma$  (68% confidence).

search fields from our best-fit  $UV$  LF (i.e.,  $M_{UV}^* = -19.8$  mag,  $\phi = 0.0011$  Mpc<sup>-3</sup>) in red and compare it against the best-fit model where  $M_{UV}^*$  shows no evolution from  $z \sim 4$  (green lines:  $M_{UV}^* = -21$ ,  $\phi^* = 0.00012$  Mpc<sup>-3</sup>). The observed surface densities of dropouts are shown with the solid histogram. As is apparent from this figure, the model with the bright value of  $M_{UV}^*$  predicts too many bright sources (e.g., ISAAC/MOIRCS panel) and too few faint sources (e.g., HUDF panel), whereas the model with a fainter value of  $M_{UV}^*$  provides a better match to the observations. The significance of this result, however, is clearly only modest ( $3\sigma$ ) at present, given the limited statistics. Better statistics would also be helpful for verifying that our treatment of the selection effects in each search field is reasonably accurate.

For our  $z \sim 9$   $J$ -dropout selection, we cannot derive a set of best-fit Schechter parameters due to the lack of any dropout candidates in our sample. Nonetheless, it does make sense for us to set constraints on  $M_{UV}^*$  and  $\phi^*$  assuming no evolution in the other Schechter parameters from  $z \sim 4$ . For example, supposing there is no evolution in  $M_{UV}^*$  (i.e.,  $M_{UV}^* = -21$ ), we can set a  $1\sigma$  upper limit of  $< 0.00006$  Mpc<sup>-3</sup> ( $\sim 20\times$  lower than at  $z \sim 4$ ) on  $\phi^*$ . Similarly, assuming there is no evolution in  $\phi^*$  (i.e.,  $\phi^* = 0.0011$  Mpc<sup>-3</sup>), we can set a  $1\sigma$  lower limit of  $-19.6$  AB mag (1.4 mag fainter than at  $z \sim 3$ ) on  $M_{AB}^*$ . The joint constraints on the value of  $\phi^*$  and  $M_{UV}^*$  are shown in Figure 5 with the black lines indicating the 68% and 95% confidence limits.

In constraining the Schechter parameters at  $z \sim 7$  and  $z \sim 9$  from our  $z$  and  $J$ -dropout searches, we assumed that the faint-end slope  $\alpha$  was equal to the same value we had previously determined at  $z \sim 6$ , i.e.,  $\alpha = -1.74$ . To see how these constraints might depend upon the assumed faint-end slope  $\alpha$ , we repeated the determinations assuming a faint-end slope  $\alpha$  of  $-1.4$  and  $-2.0$ . The results are presented in Table 5, and it is clear that the derived values for  $M_{UV}^*$  and  $\phi^*$  only show a mild dependence on the assumed faint-end slope  $\alpha$ , particularly when compared to the uncertainties on these two parameters from other error sources (e.g., from small number statistics). We can therefore essentially ignore the effect

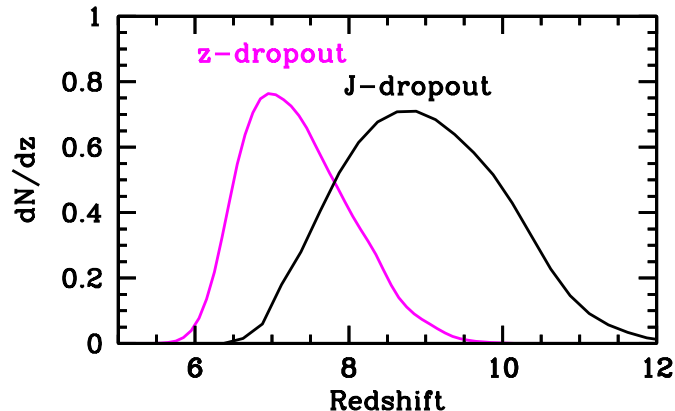


FIG. 7.— The redshift distributions predicted for our  $z$  and  $J$ -dropout selections (shown as the magenta and black lines, respectively) using our derived LFs and the simulation results presented at the beginning of §4. The  $z$ -dropout predictions assume  $M_{UV,AB} = -19.8$  and  $\alpha = -1.74$  (Table 4) while the  $J$ -dropout prediction assume  $M_{UV,AB} = -19.1$  and  $\alpha = -1.74$  (derived from the extrapolations derived in §5.3). The mean redshifts expected for our  $z$ -dropout and  $J$ -dropout selections are 7.3 and 9.0, respectively. These mean redshifts are somewhat lower than that of previous selections we had considered (e.g., Bouwens et al. 2004c; Bouwens et al. 2005; Bouwens & Illingworth 2006) because of our use of slightly more inclusive selection criteria in this work.

of the uncertain faint-end slope on our quoted constraints for both  $M_{UV}^*$  and  $\phi^*$ .

To put the LF fit results and dropout selections in context, it seems helpful to use our best-fit LFs to calculate an expected redshift distribution for our  $z$  and  $J$  dropout selections. We can take advantage of the same simulations described at the beginning of §4 to calculate these redshift distributions. For concreteness,  $M_{UV,AB}^* = -19.1$  and  $\alpha = -1.74$  are assumed for the  $UV$  LF at  $z \sim 9$  for our  $J$ -dropout selection (using the extrapolations from §5.3). The redshift distributions are presented in Figure 7. The mean redshifts expected for our  $z$ -dropout and  $J$ -dropout selections are 7.3 and 9.0, respectively. The mean redshifts estimated for both selections are smaller than what we had considered in previous works (e.g., Bouwens et al. 2004c; Bouwens et al. 2005; Bouwens & Illingworth 2006) because of our adoption of a slightly more inclusive dropout criterion in this work. Note that including the likely evolution across the redshift range of these selections would likely lower the mean redshifts even more (Muñoz & Loeb 2008).

#### 4.3. Luminosity / SFR density

We can use the present LF results to refine our constraints of the rest-frame  $UV$  luminosity densities at  $z \gtrsim 7$ . Previously, we set constraints on these quantities based upon a sample of four  $z \sim 7$   $z$ -dropout candidates found over the GOODS fields (Bouwens & Illingworth 2006) and a sample of three possible  $J$ -dropout candidates over the deep NICMOS parallels to the HUDF (Bouwens et al. 2005).

Here we are able to make modest but significant improvements in our measurement of the  $UV$  luminosity density at  $z \sim 7 - 10$ . We make these estimates based upon our best-fit LFs at  $z \sim 7$  and  $z \sim 9$ . We shall consider integrations to a limiting luminosity of  $0.2 L_{z=3}^*$  because this corresponds to the approximate flux limit for our  $z$  and  $J$ -dropout searches (i.e.,  $H_{160,AB} \sim 28$ ).

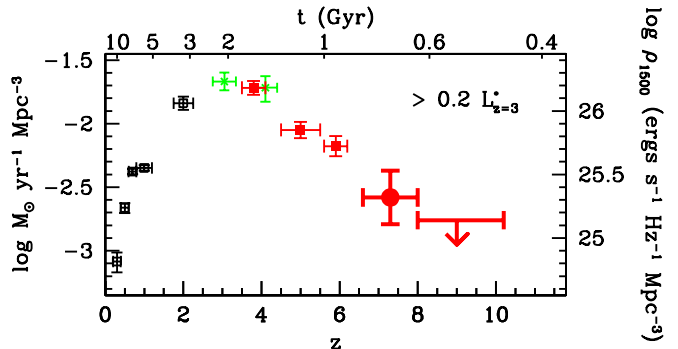


FIG. 8.— The present constraints on the  $UV$  luminosity density at  $z \gtrsim 7$ . At  $z \sim 7$ , this constraint is shown as a large solid red circle while at  $z \sim 9$ , it is shown as a  $1\sigma$  upper limit (red downward arrow). These determinations are integrated to  $0.2 L_{z=3}^*$  to match the approximate faint limits on our  $z \gtrsim 7$  galaxy searches. Also shown are the determinations of Schiminovich et al. (2005: open black squares), Steidel et al. (1999: green crosses), and Bouwens et al. (2007: solid red squares) integrated to the same flux limit.

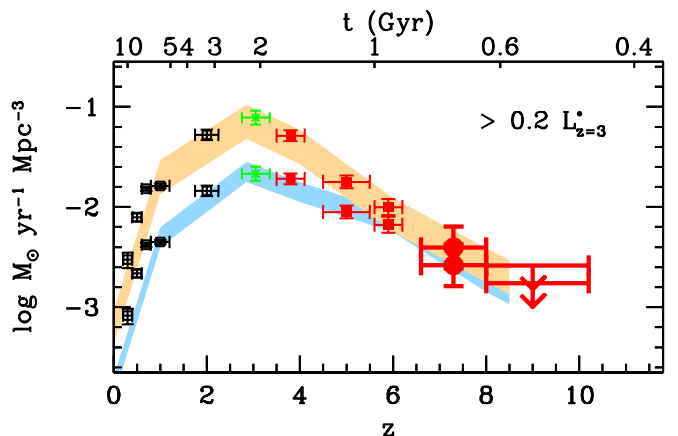


FIG. 9.— Estimated star formation rate density as a function of redshift (integrated down to  $0.2 L_{z=3}^*$  as in Figure 8). The lower set of points give the SFR density without a correction for dust extinction, and the upper set of points give the SFR density with such a correction. This is also indicated with the shaded blue and red regions, respectively, where the width of these regions show the approximate uncertainties estimated by Schiminovich et al. (2005). At lower redshift ( $z \lesssim 3$ ), we adopt the dust correction suggested by Schiminovich et al. (2005). At  $z \gtrsim 6$ , we adopt the dust correction obtained by Bouwens et al. (2006: see also Stark et al. 2007a and Stanway et al. 2005) at  $z \sim 6$  from the  $UV$ -continuum of  $i$ -dropouts and the Meurer et al. (1999) IRX- $\beta$  prescription. At  $z \sim 4$  and  $z \sim 5$ , we interpolate between the estimated dust extinctions at  $z \sim 3$  and  $z \sim 6$ . The symbols are the same as in Figure 8.

We present these luminosity densities in Figure 8 and Table 6. As is conventional, we also present the equivalent star formation rate on this same figure using the Madau et al. (1998) and adopting a Salpeter IMF. To show how this situation changes when a plausible account of dust is included, we plot the equivalent dust-corrected and uncorrected SFR densities in Figure 9. We employ the dust corrections adopted by Bouwens et al. (2007), which are 1.4 mag, 1.1 mag, 0.6 mag, and 0.4 mag at  $z \lesssim 3$ ,  $z \sim 4$ ,  $z \sim 5$ , and  $z \gtrsim 6$ , respectively. Our use of an evolving dust correction from  $z \gtrsim 6$  to  $z \sim 3$  is motivated by the apparent evolution in the  $UV$ -continuum slope over this redshift range (e.g., Stanway et al. 2005; Bouwens et al. 2006) and the correlation of  $UV$ -continuum slope with dust extinction (e.g., Meurer et al. 1999; Reddy et al.



TABLE 6  
UV LUMINOSITY DENSITIES AND STAR FORMATION RATE  
DENSITIES.<sup>a</sup>

Sample	$\langle z \rangle$	$\log_{10} \mathcal{L}$	$\log_{10}$ SFR density	
		( $\text{ergs s}^{-1}$ $\text{Hz}^{-1} \text{Mpc}^{-3}$ )	( $M_{\odot} \text{Mpc}^{-3} \text{yr}^{-1}$ ) Uncorrected	Corrected <sup>b</sup>
$z$	7.3	25.32±0.21	-2.58 ± 0.21	-2.40 ± 0.21
$J$	9.0	< 25.14 <sup>c</sup>	< -2.76 <sup>c</sup>	< -2.58 <sup>c</sup>
$B$	3.8	26.18±0.05	-1.72±0.05	-1.29 ± 0.05
$V$	5.0	25.85±0.06	-2.05±0.06	-1.75 ± 0.06
$i$	5.9	25.72±0.08	-2.18±0.08	-2.00 ± 0.08

<sup>a</sup>Integrated down to 0.2  $L_{z=3}^*$ . Based upon LF parameters in Table 4 (see §4.3).

<sup>b</sup>The adopted dust-extinction corrections are 0.4 mag, 0.6 mag, and 1.1 mag at  $z \gtrsim 6$ ,  $z \sim 5$ , and  $z \sim 4$ , respectively. Our use of an evolving dust correction from  $z \gtrsim 6$  to  $z \sim 3$  is motivated by the apparent evolution in  $UV$ -continuum slope over this redshift range (e.g., Stanway et al. 2005; Bouwens et al. 2006) and the correlation of  $UV$ -continuum slope with dust extinction (e.g., Meurer et al. 1999; Reddy et al. 2006).

<sup>c</sup>Upper limits here are  $1\sigma$  (68% confidence).

2006).

## 5. DISCUSSION

### 5.1. How does the volume density of $UV$ -bright galaxies evolve?

Over the past few years, there has been some controversy regarding how the  $UV$  LF evolves at high redshift. While some studies have argued that the evolution primarily occurs at the bright end (i.e., Dickinson et al. 2004; Shimasaku et al. 2005; Ouchi et al. 2004a; Bouwens et al. 2006; Yoshida et al. 2006; Bouwens et al. 2007), there have been other efforts which have argued that the evolution occurs primarily at the faint end (i.e., Iwata et al. 2003; Sawicki & Thompson 2006; Iwata et al. 2007). In this work, we found additional evidence to support the fact that the most rapid evolution occurs at the bright end of the  $UV$  LF and that this evolution can be approximately described by a change in the characteristic luminosity  $M_{UV}^*$  of the  $UV$  LF.

A significant part of the debate regarding the form the evolution of the  $UV$  LF takes at high redshift is centered on what happens at the bright end of the LF (i.e.,  $M_{UV,AB} \lesssim -20.5$ ). Does it evolve or not? Iwata et al. (2007) and Sawicki & Thompson (2006) argue that there is little evidence for substantial evolution from  $z \sim 5$  to  $z \sim 3$  from their work. However, a quick analysis of results in the literature indicate that such evolution is certainly very strong, particularly if the baseline is extended out to even higher redshifts ( $z \gtrsim 6$ ). At  $z \sim 6$ , for example, the bright end of the  $UV$  LF (i.e.,  $M_{UV,AB} < -20.5$ ) has been reported to be deficient by factors of  $\sim 6 - 11$  relative to  $z \sim 3 - 4$  (Stanway et al. 2003, 2004; Shimasaku et al. 2005; Bouwens et al. 2006). At  $z \gtrsim 7$ , this deficit is even larger, as we can see by comparing the number of  $UV$  bright galaxies (i.e.,  $M_{UV,AB} < -20.5$ ) in our dropout selections with that expected from  $z \sim 4$  (Bouwens et al. 2007) assuming no-evolution. The comparisons are presented in Table 7. At  $z \sim 7$ , the volume density of  $UV$  bright ( $M_{UV,AB} < -20.5$ ) galaxies appears to be  $18_{-11}^{+32} \times$  smaller than at  $z \sim 4$  (see also

TABLE 7  
COMPARISON OF THE OBSERVED NUMBERS OF DROPOUTS  
WITH NO-EVOLUTION EXTRAPOLATIONS FROM  $z \sim 4$ <sup>a</sup>

Sample	Number		Evolutionary Factor <sup>b</sup>
	Observed	$z \sim 4$ Prediction <sup>a</sup>	
Bright ( $M_{UV,AB} < -20.5$ )			
$z$ -dropout	2	35.9	$18_{-11}^{+32}$
$J$ -dropout	0	17.9	$> 16^c$
Faint ( $M_{UV,AB} > -20.5$ )			
$z$ -dropout	6	24.7	$4_{-2}^{+3}$
$J$ -dropout	0	8.0	$> 7^c$

<sup>a</sup>Extrapolations assume no evolution in the  $UV$  LF from  $z \sim 4$  (Bouwens et al. 2007) and were calculated using Eq. 1. The sizes and  $UV$  colors of  $UV$ -bright galaxies at  $z \gtrsim 7$  assumed for these estimates are the same as those given in Appendix B.

<sup>b</sup>Ratio of volume density of galaxies at  $z \sim 4$  (Bouwens et al. 2007) in some luminosity range to that in our higher redshift dropout samples.

<sup>c</sup>Lower limits here are  $1\sigma$  (68% confidence).

Bouwens & Illingworth 2006; Mannucci et al. 2007; Stanway et al. 2008), and at  $z \sim 9$ , the volume density of  $UV$  bright galaxies is at least  $16 \times$  smaller (68% confidence).

The only analysis to find mild evolution in the volume density of  $UV$  bright galaxies from  $z \sim 7 - 10$  to  $z \sim 3 - 4$  is that of Richard et al. (2006) and involves a search for  $z \geq 6$  galaxies behind lensing clusters. However, as we argue in Appendix C, it seems likely that a substantial fraction of the  $UV$ -bright galaxies in the Richard et al. (2006)  $z \sim 6 - 10$  selection are spurious and therefore the bright end of their  $UV$  LFs is much too high. The evidence for this is rather striking: not only are none of the  $z \geq 6$  candidates in the Richard et al. (2006) selection detected ( $< 2\sigma$ ) in significantly deeper ( $\sim 1-2$  mag) NICMOS+IRAC data (11 of their  $z \geq 6$  candidates), but also their reported prevalence is  $> 10 \times$  higher than what we measure in searches for similar candidates behind lensing clusters (Bouwens et al. 2008; see also Appendix C).

Considering the substantial evolution found from  $z \gtrsim 7$  to  $z \sim 4$  in the volume density of  $UV$  bright galaxies, it is certainly relevant to note that all three previous studies (i.e., Iwata et al. 2003; Sawicki & Thompson 2006; Iwata et al. 2007) which argued for less evolution at the *bright* end of the LF than at the *faint* end did not extend to redshifts much higher than 4. In fact, the very mild evolution (or no-evolution) at the bright end of LF claimed by the above studies seems to be highly consistent with other analyses in this redshift range (e.g., Steidel et al. 1999; Reddy et al. 2007) which in general find very little evolution from  $z \sim 4$  to  $z \sim 2$ . Even for the Iwata et al. (2007) LF at  $z \sim 4.7$  (which is fairly similar to the  $UV$  LFs at  $z \sim 2 - 4$  at bright luminosities), one may not expect much evolution at the bright end. After all, the mean redshift of their bright selection is  $z \sim 4.5$ , which is not much higher than  $z \sim 4$ .<sup>3</sup>

<sup>3</sup> The mean redshift for bright galaxies in the Iwata et al. (2007) selection is likely to be somewhat lower in redshift than for the fainter ones. This is because (1) the Iwata et al. (2007) selection window extends to somewhat lower redshift for the redder star-forming galaxy population than it does for the bluer star-forming galaxy population and (2) brighter star-forming galaxies at  $z \sim 4 - 6$  are observed to have much redder  $UV$  colors in general than

TABLE 8  
BEST-FIT SCHECHTER PARAMETERS FOR THE  $UV$  LFs AT  
 $z \sim 7$  AND  $z \sim 9$  ASSUMING DIFFERENT MEAN  
 $UV$ -CONTINUUM SLOPES  $\beta$ 'S TO COMPUTE THE SELECTION  
VOLUMES FOR OUR DROPOUT SAMPLES (SEE §5.2).<sup>a</sup>

Dropout Sample	$\langle z \rangle$	Mean $\beta$	$M_{UV}^*$ <sup>b</sup>	$\phi^*$ ( $10^{-3}$ Mpc $^{-3}$ )
$z$	7.3	-2.0	$-19.8 \pm 0.4$	$1.1^{+1.6}_{-0.7}$
$z$	7.3	-2.5	$-19.8 \pm 0.4$	$1.3^{+0.8}_{-0.7}$ <sup>d</sup>
$z$	7.3	-1.5	$-19.8 \pm 0.4$	$1.3^{+1.7}_{-0.8}$ <sup>d</sup>
$J$	9.0	-2.0	$> -19.6^c$	$(1.1)^e$
$J$	9.0	-2.5	$> -19.7^c$	$(1.1)^e$
$J$	9.0	-1.5	$> -19.5^c$	$(1.1)^e$

<sup>a</sup>All LFs assume a faint-end slope  $\alpha$  equal to  $-1.74$ .

<sup>b</sup>See remarks in Table 4.

<sup>c</sup>Lower limits here are  $1\sigma$  (68% confidence).

<sup>d</sup>Both bluer and redder  $UV$ -continuum slopes can result in slightly lower estimated selection volumes for star-forming galaxies at  $z \sim 7$ .

<sup>e</sup>Fixed in our fits.

In summary, it would appear that the most reasonable conclusions to draw from these studies are that the bright end of the  $UV$  LF shows substantial evolution at very high redshifts ( $z \gtrsim 4$ ) and then mild evolution at somewhat later times (i.e., from  $z \sim 4$  to  $z \sim 2$ ).

### 5.2. Completeness of current samples in $UV$ -continuum slope

The selection criteria we use to select star-forming galaxies at  $z \gtrsim 7$  (and at  $z \lesssim 6$ ) differ somewhat in the efficiency with which they select galaxies that have red  $UV$ -continuum slopes  $\beta$ , i.e.,  $\beta \gtrsim 0.0$ .<sup>4</sup> This would potentially have an effect on our determinations of the  $UV$  LFs if such red star-forming galaxies existed in large numbers. Fortunately, for these dropout selections, it appears that they do not. At  $z \sim 4$ , for example, both Lyman-break and Balmer-break selections almost entirely consist of galaxies with  $\beta$ 's bluer than  $-1.0$  (§4.1 and Figure 8 of Bouwens et al. 2007; Brammer & van Dokkum 2007). At  $z \sim 5 - 6$ , the galaxy population appears to be bluer yet, with mean  $\beta$ 's of  $\sim -2$  (e.g., Stanway et al. 2005; Bouwens et al. 2006; Yan et al. 2005; Lehnert & Bremer 2003; Hathi et al. 2008), and there is little evidence from the present selections that the galaxy population is any less blue at  $z \gtrsim 7$ . Indeed, the observed  $J_{110} - H_{160}$  colors are consistent with a

the fainter star-forming galaxies at these redshifts (e.g., Meurer et al. 1999; Iwata et al. 2007; R.J. Bouwens et al. 2008, in prep). As a result, the mean redshift for bright galaxies in the Iwata et al. (2007) selection will be lower than for the faint galaxies, and therefore the bright end of the Iwata et al. (2007) LF should show less evolution than the faint end.

<sup>4</sup> For our  $z$ -dropout selection, for example, we would only be moderately effective at selecting galaxies with  $UV$ -continuum slopes  $\beta$  redder than  $\beta = 0$  (Figure 2). For our  $J$ -dropout selection, on the other hand, there is no limit on how red a star-forming galaxy can be in terms of its  $UV$ -continuum slope, except as set by our restrictions on the IRAC and MIPS colors of sources (i.e.,  $3.6\mu - 5.8\mu < 1$ ,  $3.6\mu - 24\mu < 2$ : see §3.2) which require  $\beta \lesssim 0$ . For the Bouwens et al. (2007)  $z \sim 4$   $B$ -dropout,  $z \sim 5$   $V$ -dropout, and  $z \sim 6$   $i$ -dropout selections, we are only effective in selecting star-forming galaxies, if their  $UV$ -continuum slopes  $\beta$  are bluer than  $\beta = 0.5$  (see Figure 8 of Bouwens et al. 2007).

star-forming population with little dust and  $10^8$  years of constant star formation (where  $\beta \sim -2$ : see Figure A1).

Of course, even if our dropout selections are largely complete in their selection of dropouts over a wide range in  $UV$ -continuum slope, it is possible that the  $UV$  LF we derive may depend somewhat on the distribution of  $UV$  continuum slopes we are using to model the selection volumes for our high-redshift dropout samples. We would not expect the distribution we are assuming to be too inaccurate, as we are able to use this distribution to reproduce the observed  $J_{110} - H_{160}$  colors of our  $z$ -dropout sample (Appendix B: see Figure A1). Nonetheless, it is worthwhile examining the sensitivity of our results to small changes in the distribution of  $UV$ -continuum slopes  $\beta$ . Bouwens et al. (2007) examined the effect that different assumptions about these slopes would have on the  $UV$  LF at  $z \sim 4 - 6$  and found changes of  $\lesssim 10\%$  in the fit parameters for shifts of 0.7 in the mean  $UV$ -continuum slope  $\beta$ . Repeating our determinations of the  $UV$  LF at  $z \sim 7$  and  $z \sim 9$  assuming a mean  $UV$ -continuum slope of  $-2.5$ , we find differences of  $\lesssim 20\%$  in the constraints on  $M^*$  and  $\phi^*$  (Table 8). Similarly small differences were found relative to previous fits assuming a mean  $UV$ -continuum slope  $\beta$  of  $-1.5$  (Table 8). This suggests that our LF fit results are relatively robust with respect to uncertainties about the distribution in  $UV$ -continuum slopes  $\beta$ .

### 5.3. Evolution of the LF

In this work, we derived constraints on the  $UV$  LF at  $z \sim 7$  and  $z \sim 9$  using both a stepwise and Schechter parametrization. For our Schechter parametrization, we estimated that the value of  $M_{UV}^*$  for the  $UV$  LF at  $z \sim 7$  was equal to  $-19.8 \pm 0.4$  mag and  $\phi^* = 0.0011^{+0.0017}_{-0.0007}$  Mpc $^{-3}$ . The value of  $M_{UV}^*$  we derived at  $z \sim 7$  is  $0.4 \pm 0.4$  mag fainter than we found at  $z \sim 6$ . This is consistent with the trend previously discovered over the redshift interval  $z \sim 4 - 6$  where the value of  $M_{UV}^*$  was fainter the earlier back in time we probed (see also Yoshida et al. 2006). We have already remarked that the value of  $\phi^*$  is quite consistent with the values found at  $z \sim 4$ ,  $z \sim 5$ , and  $z \sim 6$  by Bouwens et al. (2007: see also Yoshida et al. 2006). We also attempted to constrain the Schechter parameters at  $z \sim 9$  using the results of our  $J$ -dropout search. Assuming that we can model the changes in the  $UV$  LF from  $z \sim 9$  using a Schechter function and that these changes can be parametrized by an evolution in  $M_{UV}^*$  (with  $\phi^*$  and  $\alpha$  fixed, as is suggested by our constraints on the  $UV$  LF from  $z \sim 4$  to  $z \sim 7$ ), we found that  $M_{UV, z=10}^* > -19.6$  mag (68% confidence). Plotting the constraints on  $M_{UV}^*$  versus redshift (Figure 10), it seems clear that the observations are consistent with a substantial brightening of  $M_{UV}^*$  at early cosmic times. The brightening of  $M_{UV}^*$  is  $> 1.4$  mag from  $z \sim 9$  to  $z \sim 4$ . This, of course, is in contrast to the behavior of  $M_{UV}^*$  at  $z \lesssim 4$  where  $M_{UV}^*$  reaches a maximum brightness at  $z \sim 2 - 4$  and then fades with cosmic time (e.g., Gabasch et al. 2004; Arnouts et al. 2005).

We can put together the constraints on the  $UV$  LF from  $z \sim 7 - 10$  to  $z \sim 4$  (i.e., Figure 5 from this work and Figure 3 from Bouwens et al. 2007) to derive approximate expressions for  $M_{UV}^*$ ,  $\phi^*$ , and  $\alpha$  as a function of redshift (at  $z \gtrsim 4$ ). Assuming that the dependence of

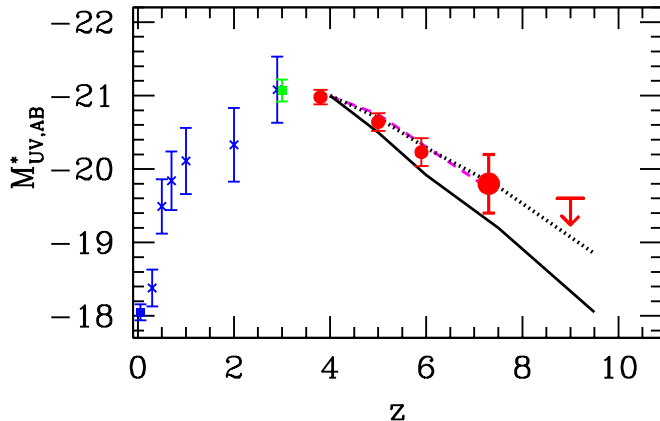


FIG. 10.— Determinations of the characteristic luminosity  $M^*$  in the rest-frame  $UV$  as a function of redshift. Shown are our present determination at  $z \sim 7$  (large red circle) and  $1\sigma$  upper limit at  $z \sim 9$  (red downward arrow). Also included are the determinations at  $z \sim 4$ ,  $z \sim 5$ , and  $z \sim 6$  from Bouwens et al. (2007: red circles), at  $z \sim 3$  from Steidel et al. (1999: green cross), and at  $z \lesssim 3$  from Arnouts et al. (2005: blue crosses), and at  $z \sim 0$  from Wyder et al. (2005: blue square). The expected evolution in  $M^*$  predicted from the momentum-driven wind “vzw” model of Oppenheimer & Davé (2006) is plotted as the dashed magenta line while the evolution expected as a result of a build-up in the mass function is shown. The solid black line shows the evolution predicted from the halo mass function (Sheth & Tormen 1999) assuming a mass-to-light ratio which is constant while the dotted black line shows this evolution assuming a mass-to-light ratio which varies as  $(1+z)^{-1}$  (which is somewhat less than the  $(1+z)^{-1.5}$  scaling of the mass-to-light ratio used in Wyithe & Loeb 2006 or Stark et al. 2007c: see §5.4). The predicted evolution in  $M_{UV}^*$  is derived from the models by examining the changes in the LF (or mass function) at a fixed volume density  $\sim 10^{-2.5} \text{ Mpc}^{-3}$ . The above predictions differ from those given in Bouwens et al. (2007) due to our use of a more current input matter power spectrum (Spergel et al. 2007). The observed evolution in  $M_{UV}^*$  appears to be in reasonable agreement with what one might expect from the evolution of the halo mass function, assuming an evolution in the mass-to-light ratio for halos of  $\sim (1+z)^{-1}$ .

these parameters on redshift can be parametrized in a linear way and moreover that the the  $UV$  LF can be represented by a Schechter function at  $z \gtrsim 7$  (see discussion in §5.5), we derive the following relationships for  $M_{UV}^*$ ,  $\phi^*$ , and  $\alpha$  for  $z \sim 4 - 7$ :

$$\begin{aligned} M_{UV}^* &= (-21.02 \pm 0.09) + (0.36 \pm 0.08)(z - 3.8) \\ \phi^* &= (1.16 \pm 0.20)10^{(0.024 \pm 0.065)(z - 3.8)}10^{-3} \text{ Mpc}^{-3} \\ \alpha &= (-1.74 \pm 0.05) + (0.04 \pm 0.05)(z - 3.8) \end{aligned}$$

These equations provide us with a convenient way of extrapolating our observational results back to early times (i.e.,  $z > 7$ ). They also provide us with a very quantitative way of assessing the significance of the evolutionary trends identified in  $M_{UV}^*$ ,  $\phi^*$ , and  $\alpha$ . In particular, these equations suggest that the observed evolution in  $M_{UV}^*$  is significant at the  $4.5\sigma$  level over the interval  $z \sim 9$  to  $z \sim 4$ , while the evolution in  $\phi^*$  and  $\alpha$  is still not significant at all (i.e.,  $< 1\sigma$ ).

#### 5.4. Relation to the Halo Mass Function

The rapid brightening of galaxies within the first two billion years of the universe is not particularly surprising since it is during this time period that  $L^*$  galaxy halos (typically  $10^{10}$  to  $10^{12} M_\odot$ : e.g., Cooray 2005; Lee et al. 2006; Ouchi et al. 2004b; Cooray & Ouchi 2006) are largely assembled. The volume density of  $\sim 10^{11}$

$M_\odot$  halos is expected to increase 1000 fold from  $z \sim 10$  to  $z \sim 3 - 4$  (see, e.g., Figure 2 of Springel et al. 2005). Larger increases are expected at  $\gtrsim 10^{11} M_\odot$ , and smaller increases are expected at  $\lesssim 10^{11} M_\odot$ . Thus, if the efficiency of star formation in galaxies does not decrease substantially as a function of cosmic time, we would expect substantial increases in the volume density of luminous star-forming galaxies from  $z \sim 9$  to  $z \sim 4$ . We would also expect the maximum typical luminosity of star-forming galaxies (and thus  $M_{UV}^*$ ) to increase over this time period (due to the greater evolution expected for more massive galaxies). This is exactly what our LFs suggest (Figure 10).

In light of these expectations, it is relevant to try to connect the evolution we observe in the rest-frame  $UV$  LF to the anticipated changes in the halo mass function. Not only does this provide us with a simple test of our theory for structure formation, but it also allows us to place modest constraints on the efficiency with which halos in the early universe produce  $UV$  photons.

In our previous work (§5.2 of Bouwens et al. 2007), we decided to parametrize the evolution in the  $UV$  LF and that expected for the halo mass function in terms of a single variable for simplicity. Motivated by our observational findings (Bouwens et al. 2006; Bouwens et al. 2007), we took this parameter to be the characteristic luminosity for our  $UV$  LF and some characteristic mass for the halo mass function. The characteristic mass was taken to equal the mass where the mass function had a comoving volume density of  $10^{-2.5} \text{ Mpc}^{-3}$  to (approximately) match the volume density of  $\phi^*$  galaxies. We ignored questions about a possible evolution in the shape of the  $UV$  LF or mass function.<sup>5</sup> Making different assumptions about how the mass-to-light ratio (halo mass to  $UV$  light) of halos vary as a function of redshift, we developed predictions for how  $M_{UV}^*$  might be expected to change with redshift – assuming a matter power spectrum with  $\sigma_8 = 0.9$ , spectral index  $n_s = 1$ ,  $\Omega_M = 0.3$ ,  $\Omega_\Lambda = 0.7$ , and  $H_0 = 70 \text{ km/s/Mpc}$ . We found that the observations seemed to prefer a scenario where there was little evolution in the mass-to-light ratio of halos at early times.

Given the similarity of the present observational results to those previously considered by Bouwens et al. (2007), one might suspect that the above conclusions would remain unchanged. However, after exploring the sensitivity of these conclusions to different inputs, we found that they could depend significantly upon assumptions made in calculating the halo mass function. In particular, we found that for the matter power spectrum preferred by the WMAP three year data and the SDSS large-scale structure constraints ( $\sigma_8 = 0.772$ ,  $n_s = 0.948$ ), the evolution we predicted for the characteristic mass was  $\sim 40\%$  larger than what we predicted in our previous work using  $\sigma_8 = 0.9$  and  $n_s = 1$ . This translated into a  $\sim 40\%$  larger predicted brightening of  $M_{UV}^*$  with cosmic time than in the previous predictions, and so as a result our models with no evolution in the mass-to-light ratio (halo mass to  $UV$  light) were no longer in good agreement with the

<sup>5</sup> We note that we find very similar changes in the so-called characteristic mass here if we make the comparisons in terms of the average (or even median) mass of halos at the high-mass end of the mass function ( $\lesssim 10^{-2.5} \text{ Mpc}^{-3}$ ).

observations (see solid line in Figure 10).

We therefore explored different scalings of the mass-to-light ratio of halos to try to regain good agreement with the observations. We found reasonable agreement, adopting a halo mass-to-light ratio that varied as  $(1+z)^{-1}$  (see dotted line in Figure 10). Such a scaling would mean that star formation at early times is much more efficient than at later times and, in fact, does not scale that differently from what one would expect based upon the dynamical time scales (which evolves as  $\sim (1+z)^{-1.5}$ : e.g., Wyithe & Loeb 2006; Stark et al. 2007c). Of course, it seems prudent to remember that these conclusions are likely highly uncertain. They are clearly somewhat sensitive to the input matter power spectrum that one adopts, and it seems likely that there are other uncertainties that will have an effect (e.g., the issues discussed in §5.5).

### 5.5. Shape of the UV LFs at $z \gtrsim 4$

Of course, the UV LFs we have derived at  $z \gtrsim 4$  contain a lot more information than is present in a single parameter. They also contain substantial information on the overall shape of the UV LF. Perhaps the most notable feature in the shape of the observed LFs at  $z \sim 4$ ,  $z \sim 5$ , and  $z \sim 6$  is the presence of a distinct “knee,” where the LF transitions from a power-law-like behavior towards fainter magnitudes to an exponential cut-off at the bright end. At lower redshifts, this exponential cut-off at the bright end of the LFs is well-known and has been hypothesized to occur as a result of a variety of different factors. Classically, this cut-off has been explained as a result of the inefficiency with which gas can cool in halos above  $10^{12} M_{\odot}$  (e.g., Binney 1977; Rees & Ostriker 1977; Silk 1977) and settle out of hydrostatic equilibrium. This explanation has recently been updated and recast in terms of a discussion of hot and cold flows (i.e., Birnboim & Dekel 2003; Dekel & Birnboim 2004). The exponential cut-off at the bright end of the LF has also been explained as a result of AGN feedback (e.g., Binney 2004; Scannapieco & Oh 2004; Croton et al. 2006; Granato et al. 2004), which above a certain mass scale is thought to cut off the flow of cold gas to a galaxy and therefore stop star formation. One final factor which may be important for imparting the sharp cut-off at the bright end of the LF, particularly at UV wavelengths, is dust obscuration, which becomes substantial (factors  $\gtrsim 10$ ) for the most luminous systems (e.g., Wang & Heckman 1996). As a result, the UV luminosity of star-forming galaxies does not tend to reach above some maximum value (see discussion in e.g., Adelberger & Steidel 2000; Martin et al. 2005).

At very high redshifts, where the typical halo masses are smaller, none of the above mechanisms would seem to work very well. The typical masses are below those where AGN feedback might be expected to be important (e.g., Scannapieco & Oh 2004; Dekel & Birnboim 2004) or where gas cooling is inefficient (i.e.  $< 10^{12} M_{\odot}$ : Dekel & Birnboim 2004).<sup>6</sup> The expected star-formation rates at these redshifts would also tend to be much lower and therefore dust obscuration would not likely be such an

<sup>6</sup> Nonetheless, it has been argued (e.g., Dekel & Birnboim 2004) that at  $z > 2$  gas cooling will occur very efficiently in some regions of high mass ( $\gtrsim 10^{12} M_{\odot}$ ) halos through “cold flows.”

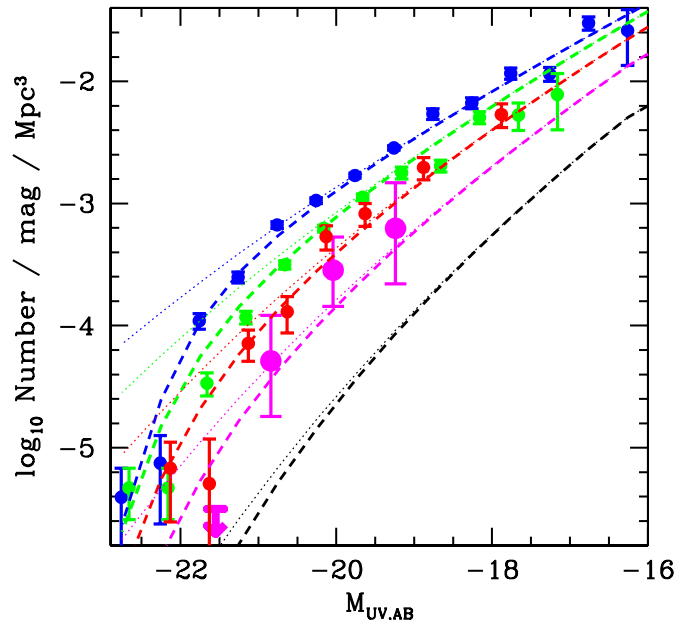


FIG. 11.— Rest-frame UV LFs predicted at  $z \sim 4$ ,  $z \sim 5$ ,  $z \sim 6$ ,  $z \sim 7$ , and  $z \sim 9$  (dashed blue, green, red, magenta, and black lines, respectively) using a CLF formalism (see §5.5) compared with those from our observations. The stepwise LFs found in the observations are presented in the same way as in Figure 4. The CLF kernel used to convert mass into light was chosen to fit the LF at  $z \sim 4$ . The predicted LFs using a kernel with no cut-off at the bright end of the mass function is shown using the dotted line (i.e., assuming  $L_c(M) = (2.51 \times 10^{22} \text{ W Hz}^{-1})(M/m_c)^{1.24}$ ). At  $z \gtrsim 4$ , we adopt the same CLF kernels as at  $z \sim 4$  to calculate the UV LF from the halo mass function, but modified to include the  $\sim (1+z)^{-1}$  evolution in the mass-to-light ratio inferred by comparing the UV LFs with the expected halo mass function (see Figure 10). The LFs predicted using these assumptions do not show an extremely prominent “knee” so characteristic of “typical” Schechter functions at  $z \geq 6$ .

important factor either (given the correlation between these two quantities: e.g., Wang & Heckman 1996). As such, it would seem that there are no obvious mechanisms to impose an abrupt cut-off at the bright end of the UV LF and therefore we might expect that the UV LFs at very early times ( $z \gtrsim 6$ ) to lack the “knee” so characteristic of the Schechter parametrization and look much more like the mass function. In fact, the UV LFs at  $z \gtrsim 4$  derived from a number of recent theoretical simulations (e.g., Figure 7 of Finlator et al. 2006; Figure 10 of Oesch et al. 2007) have exactly those characteristics. Those predicted LFs bear a much closer resemblance to power laws than they do to the traditional Schechter function. The observation of a significant knee-or cut-off-at the bright end of the observed LFs out to  $z \sim 6$  may mean that there is some additional physics relevant to the formation of galaxies that is not fully understood.

*Conditional Luminosity Functions:* To illustrate this issue quantitatively, we adopt a simplified version of the conditional luminosity function (CLF) formalism laid out in Cooray & Ouchi (2006: see also Yang et al. 2003; Cooray & Milosavljević 2005). The CLF formalism provides us with a way of converting some halo mass function to a LF. Typically there is a kernel which when convolved with the mass function gives the LF, i.e.,

$$\phi(L) = \int_M \phi(L|M) \frac{dN}{dM} dM$$

where

$$\phi(L|M) = \frac{1}{\sqrt{2\pi}(\log_e 10)\sigma L} \times \exp\left\{-\frac{\log_{10}[L/L_c(M)]^2}{2\sigma^2}\right\}$$

where  $\frac{dN}{dM}$  is the Sheth-Tormen (1999) mass function, where  $\log_e 10 \approx 2.303$ , where  $L_c(M)$  gives the  $UV$  luminosity of the central galaxy in some halo of mass  $M$  and where the parameter  $\sigma$  expresses the dispersion in the relationship between the halo mass and the  $UV$  light of the central galaxy. Note that we have ignored the contribution from satellite galaxies to the luminosity function in the above equation since they appear to constitute  $\lesssim 10\%$  of the galaxies over a wide-range in luminosity (see, e.g., Cooray & Ouchi 2006). One aspect about the CLF formalism is that it is largely independent of much of the normal phenomenology associated with galaxy formation and therefore it is very clean. There is no attempt to explicitly model the large number of physical processes likely to be important in the formation and evolution of galaxies (which remain a challenge for most semi-analytic prescriptions, e.g., Somerville & Primack 1999; Cole et al. 2000).

Making use of the above formalism, we experimented with a variety of different parameterizations to find a function  $L_c(M)$  and parameters  $\sigma$  and  $m_c$  which reproduced the Bouwens et al. (2007)  $UV$  LF at  $z \sim 4$ . We found that  $L_c(M) = (2.51 \times 10^{22} \text{ W Hz}^{-1}) \frac{(M/m_c)^{1.24}}{(1+(M/m_c))}$ ,  $\sigma = 0.16$ , and  $m_c = 1.2 \times 10^{12} M_\odot$  worked reasonably well (see the blue dashed line in Figure 11).  $2.51 \times 10^{22} \text{ W Hz}^{-1}$  is equivalent to  $-21.91 \text{ AB mag}$ . We adopted the best-fit values of  $\sigma_8$ ,  $n_s$ ,  $\Omega_m$ ,  $\Omega_\Lambda$ ,  $\Omega_b$ , and  $h$  to the WMAP three year + SDSS data (Spergel et al. 2007). Our choice of  $m_c$  set the mass scale where the exponential cut-off in the luminosity function takes effect. At the high mass end of the mass function, our equation for  $L_c$  asymptotes towards a  $(M/m_c)^{0.2}$  behavior. The physical motivation for this cut-off at the bright-end of the mass function would presumably be the same as at low redshift, where star formation is not as efficient for the most massive halos because of inefficient gas cooling or AGN feedback. To show the effect the high mass cutoff has on the model LF, we also show this LF without such a cut-off (see the dotted lines in Figure 11). At the low-mass end, our equation for  $L_c$  asymptotes towards a  $(M/m_c)^{1.24}$  behavior. This allowed us to account for the fact that the faint-end slope of the  $UV$  LF is slightly shallower than that of the mass function (i.e.,  $-1.7$  vs.  $-2.0$ ). The chosen parameters yield similar, albeit slightly lower, halo masses to those inferred from clustering analyses of star-forming galaxies at  $z \sim 4$  (e.g., Ouchi et al. 2004b; Lee et al. 2006).

The question now is whether the above relationship between  $UV$  light and halo mass (i.e., the kernel  $\phi(L|M)$ ) can reproduce the rest-frame  $UV$  LF at  $z \gtrsim 4$ . Given the reasonable agreement between the observed evolution in  $M_{UV}^*$  and that predicted from the halo mass function assuming  $\sim (1+z)^{-1}$  in the mass-to-light ratio, one might expect that the above kernel may work if we multiply the  $L_c(M)$  expression above to include the factor  $(\frac{1+z}{1+3.8})$ . With this change,  $L_c(M)$  equals  $(2.51 \times 10^{22} \text{ W Hz}^{-1}) \frac{(M/m_c)^{1.24}}{(1+(M/m_c))} (\frac{1+z}{1+3.8})$ . The  $UV$  LFs we

predict at  $z \sim 5$ ,  $z \sim 6$ ,  $z \sim 7$ , and  $z \sim 9$  are presented in Figure 11 as the green, red, magenta, and black dashed lines, respectively. These LFs appear to differ somewhat in overall shape from what is found in our observations, predicting somewhat fewer galaxies at fainter luminosities than are observed, particularly near the “knee” of the LF (i.e., at  $\sim -19.5 \text{ AB mag}$ ). Most notably, the sharp jump in the volume densities of sources observed between the bright end of the LF (i.e.,  $\sim -22 \text{ AB mag}$ ) and the “knee” of the LF (i.e.,  $\sim -20 \text{ AB mag}$ ) is not well matched by the predicted LFs at  $z \gtrsim 6$ .

This effectively illustrates what we were describing above. To obtain a LF with a prominent “knee,” we require some physical mechanism which will truncate the LF above some luminosity (or mass). Since this “knee” of the LF would seem to shift to much fainter luminosities at early cosmic times (assuming that the evolution of the  $UV$  LF can be effectively parametrized in terms of  $M_{UV}^*$  to  $z \sim 9$  as suggested by Figure 10 or Eq. 3), this mechanism needs to become important at progressively lower luminosities (and also lower masses), as we move back in cosmic time. This is in contrast to the assumptions we use in the formalism above, where we have assumed that the mass cut-off  $m_c$  is independent of cosmic time. It is not clear that any of the mechanisms proposed to produce a cut-off at the bright end of the LF (e.g., AGN feedback, dust extinction, inefficient gas cooling at high masses) will extend to very low luminosities (or masses). The observations may therefore present us with a bit of puzzle. Alternatively, it is also possible given the observational uncertainties that the  $UV$  LFs at  $z \gtrsim 7$  will increasingly look like the halo mass function and less like a Schechter function with a prominent “knee.”

## 6. SUMMARY

We have taken advantage of all the deep near-IR and optical data that are currently public over and around the two GOODS fields (including the HUDF) to search for  $z \gtrsim 7$   $z$  and  $J$ -dropout candidates. In total, we make use of  $\sim 23 \text{ arcmin}^2$  of deep NICMOS data and  $\sim 248 \text{ arcmin}^2$  of deep ACS+ISAAC/MOIRCS data. Over these areas, we identify 8  $z$ -dropout candidates, but no plausible  $J$ -dropout candidates. By exploring all reasonable sources of contamination (T-dwarfs, high-redshift supernovae, photometric scatter, spurious sources) for our modest  $z$ -dropout sample, we argue that the majority of sources in our selection ( $\gtrsim 88\%$ ) are bona-fide star-forming galaxies at  $z \sim 7$ . Using the size-redshift trends,  $UV$  colors, and spatial profiles of star-forming galaxies at  $z \sim 4 - 6$ , we make plausible estimates of the selection volume for identifying  $z \sim 7$   $z$ -dropouts and  $z \sim 9$   $J$ -dropouts. We then use these samples and selection volumes to derive the LF at  $z \sim 7$  and set constraints on the LF at  $z \sim 9$ . We consider both stepwise and Schechter parameterizations for the  $UV$  LF.

Our primary conclusions are:

(1) *UV LF at  $z \sim 7$* : The rest-frame  $UV$  LF shows significant evolution from  $z \sim 7$  to  $z \sim 6$  (99% confidence). Our best-fit  $\phi^*$  and  $M_{UV}^*$  for the  $UV$  LF at  $z \sim 7$  is  $0.0011_{-0.0007}^{+0.0017} \text{ Mpc}^{-3}$  and  $-19.8 \pm 0.4 \text{ mag}$ , respectively, adopting the same value for the faint-end slope  $\alpha$  ( $-1.74$ ) that we previously found at  $z \sim 6$ . This value of  $M_{UV}^*$  is nearly  $1.2 \pm 0.4 \text{ mag}$  fainter than the value of  $M_{UV}^*$  that has previously been found at  $z \sim 4$  and  $0.4 \pm 0.4 \text{ mag}$



fainter than the value found at  $z \sim 6$ . By contrast, the value of  $\phi^*$  that we determined at  $z \sim 7$  is not significantly different from those values determined at slightly later times ( $z \sim 4 - 6$ ; Bouwens et al. 2007). Similar to several previous studies (Bouwens et al. 2006; Yoshida et al. 2006; Bouwens et al. 2007), this suggests that the evolution of the  $UV$  LF at  $z \gtrsim 4$  can largely be described by an evolution in the characteristic luminosity  $M_{UV}^*$ , with no significant changes required in the other variables.

(2) *Constraints on the UV LF at  $z \sim 9$* : Since we did not find any credible  $J$ -dropout candidates in our search fields, we were not able to derive best-fit parameters for the  $UV$  LF at  $z \sim 9$  and could only set constraints on  $\phi^*$  and  $M_{UV}^*$ . To interpret the implications of our  $J$ -dropout search results for the  $UV$  LF at  $z \sim 9$ , we assumed that the value of  $\phi^*$  and  $\alpha$  there were roughly equal to the values (i.e.,  $0.0011 \text{ Mpc}^{-3}$  and  $-1.74$ ) found at  $z \sim 4 - 8$ . We then derived lower limits on the value of  $M_{UV}^*$  by using our  $J$ -dropout search results and the effective selection volumes we calculated for  $z \sim 9$  galaxies using numerous Monte-Carlo simulations. We found that  $M_{UV}^* > -19.6$  mag at 68% confidence. These search constraints are inconsistent with no evolution from  $z \sim 9$  to  $z \sim 7$  at 80% confidence.

(3) *Evolution in the volume density of UV-bright galaxies*: Comparing the no-evolution predictions of the Bouwens et al. (2007)  $z \sim 4$  UV LF at bright magnitudes with those observed in the ISAAC, MOIRCS, or NICMOS data (see Table 7: see §5.1), we estimated that the bright end ( $M_{UV,AB} < -20.5$ ) of the  $UV$  LF is at least  $18_{-10}^{+32} \times$  lower at  $z \sim 7$  than it is at  $z \sim 4$ . Making a similar comparison between the number of  $J$ -dropouts predicted assuming no evolution from  $z \sim 4$  and the zero candidates found in our NICMOS search fields, we estimated that the bright end of the LF ( $M_{UV,AB} < -20.5$ ) is at least  $16 \times$  lower at  $z \sim 9$  than it is at  $z \sim 4$  (68% confidence). This provides strong evidence against evolutionary models with little evolution at the bright end of the  $UV$  LF.

(4) *Empirical fit to the UV LF from  $z \sim 9$  to  $z \sim 4$* : Putting together our constraints on the  $UV$  LF from  $z \sim 9$  to  $z \sim 4$ , we derived fitting formula to describe the evolution of  $M_{UV}^*$ ,  $\phi^*$ , and  $\alpha$  as a function of redshift. The results are  $M_{UV}^* = (-21.02 \pm 0.09) + (0.36 \pm 0.08)(z - 3.8)$ ,  $\phi^* = (1.16 \pm 0.20)10^{(0.024 \pm 0.065)(z - 3.8)}10^{-3} \text{ Mpc}^{-3}$ , and  $\alpha = (-1.74 \pm 0.05) + (0.04 \pm 0.05)(z - 3.8)$ . These formulae imply that the evolution in  $M_{UV}^*$  is significant at the  $4.5\sigma$  level. The evolution in  $\phi^*$  and  $\alpha$  is not yet significant.

(5) *Relationship between the evolution of the UV LF at  $z \gtrsim 4$  and that expected for the halo mass function*: The evolution we observe in the characteristic luminosity  $M_{UV}^*$  versus redshift matches the evolution expected for the halo mass function, assuming that the mass-to-light ratio (halo mass to UV light) of halos evolves as  $\sim (1+z)^{-1}$  with cosmic time. This finding is somewhat different from what Bouwens et al. (2007) inferred about the mass-to-light ratios of halos based upon very similar observational constraints. The reason for the change is our use of more current constraints on the matter power spectrum (i.e.,  $\sigma_8 = 0.772$ , spectral index  $n_s = 0.948$ ; Spergel et al. 2007) rather than the  $\sigma_8 = 0.9$ ,  $n_s = 1$  power spectrum we were assuming in Bouwens et al.

(2007). Effectively, this illustrates how sensitive galaxy evolution can be at high-redshift to the input matter power spectrum.

(6) *Shape of the UV LF at  $z \gtrsim 4$* : At redshifts as early as  $z \sim 6$ , the  $UV$  LF is remarkably well-represented by a Schechter function (Bouwens et al. 2007). The position of the “knee” of the LF is known to  $\lesssim 0.2$  mag at  $z \lesssim 6$  (Bouwens et al. 2007) and would seem to be known to  $\lesssim 0.4$  mag at  $z \sim 7$ . However, it is unclear why the  $UV$  LF would show a prominent knee at such early times. Most of the physical mechanisms thought to create this knee in the LF at lower redshifts (e.g., AGN feedback or a post-virialization cooling condition) would not seem to be effective at the lower masses relevant at these times.

The constraints we have on the  $UV$  LF at  $z \gtrsim 7$  are already quite notable, especially given the significant challenges that exist to the detection of  $z \gtrsim 7$  galaxies with current observational facilities. Putting together all the data now available, we can plausibly determine the volume density of  $UV$ -bright galaxies at  $z \sim 7$  to within a factor of 2 and set meaningful constraints on the volume density of similarly luminous galaxies at  $z \sim 9$ . Comparing the present search results with those obtained at lower redshift ( $z \sim 4 - 6$ ), we observe a rather substantial increase in the volume density of most luminous  $UV$ -bright galaxies, from redshifts  $z \gtrsim 7$  to  $z \sim 4$  – suggesting that such luminous and likely prodigious star-forming systems only start to become common relatively late in cosmic time (i.e., 1.5 Gyr after the Big Bang). These galaxies are presumably built up through the merging and coalescence of lower mass galaxies.

Over the next year, we expect our constraints on the bright end of  $UV$  LF at  $z \gtrsim 7$  to improve substantially as a result of both ground and space-based imaging programs. From the ground, these improvements will come as a result of the deep wide-area imaging being obtained over the GOODS fields with wide-area near-IR imagers such as MOIRCS on Subaru telescope and HAWK-I on VLT-Yepes. From space, these improvements will come from two large-to-medium-sized HST NICMOS programs (GO-11082 and GO-11144 are surveying  $\sim 60 \text{ arcmin}^2$  to a depth of  $\sim 26.5$  AB). Of course, for truly significant advances in the size and depth of current samples, we will need to wait until late 2008 when WFC3 with its powerful IR channel will be installed on the Hubble Space Telescope.

We would like to thank Louis Bergeron, Susan Kassim, Dan Magee, Massimo Stiavelli, and Rodger Thompson for their assistance in the reduction of NICMOS data which has been essential to find and characterize faint star-forming galaxies at  $z \gtrsim 7$ . We acknowledge stimulating conversations with Peter Capak, Michele Cirasuolo, Asantha Cooray, Romeel Davé, James Dunlop, Richard Ellis, Kristian Finlator, Brad Holden, Cedric Lacey, Ross McLure, Pascal Oesch, Masami Ouchi, Naveen Reddy, Piero Rosati, and Daniel Stark. We are grateful to Kristian Finlator for his continuing helpfulness in computing rest-frame  $UV$  LFs at  $z \gtrsim 4$  from his group’s theoretical models. Ivo Labbé provided us with a very deep 38-hour reduction of the VLT and Magellan  $K_s$  band imaging data over the HUDF. We thank Pascal Oesch and Li Xin for a careful read of our

## REFERENCES

- Adelberger, K. L. & Steidel, C. C. 2000, *ApJ*, 544, 218  
 Arnouts, S., et al. 2005, *ApJ*, 619, L43  
 Baba, H., et al. 2002, *Astronomical Data Analysis Software and Systems XI*, 281, 298  
 Beckwith, S. V. W., et al. 2006, *AJ*, 132, 1729  
 Bertin, E. and Arnouts, S. 1996, *A&AS*, 117, 39  
 Binney, J. 1977, *ApJ*, 215, 483  
 Binney, J. 2004, *MNRAS*, 347, 1093  
 Birnboim, Y., & Dekel, A. 2003, *MNRAS*, 345, 349  
 Bouwens, R., Broadhurst, T. and Silk, J. 1998a, *ApJ*, 506, 557  
 Bouwens, R., Broadhurst, T. and Silk, J. 1998b, *ApJ*, 506, 579.  
 Bouwens, R., Broadhurst, T., & Illingworth, G. 2003, *ApJ*, 593, 640  
 Bouwens, R. J., et al. 2004a, *ApJ*, 606, L25  
 Bouwens, R. J., Illingworth, G.D., Blakeslee, J.P., Broadhurst, T.J., & Franx, M. 2004b, *ApJ*, 611, L1  
 Bouwens, R. J., et al. 2004c, *ApJ*, 616, L79  
 Bouwens, R. J., Illingworth, G.D., Thompson, R.I., & Franx, M. 2005, *ApJ*, 624, L5  
 Bouwens, R. J., & Illingworth, G. D. 2006, *Nature*, 443, 189.  
 Bouwens, R.J., Illingworth, G.D., Blakeslee, J.P., & Franx, M. 2006, *ApJ*, 653, 53  
 Bouwens, R. J., Illingworth, G. D., Franx, M., & Ford, H. 2007, *ApJ*, 670, 928  
 Bouwens, R. J., et al. 2008, *ApJ*, submitted, arXiv:0805.0593  
 Bradley, L.D., et al. 2008, *ApJ*, 678, 647  
 Brammer, G. B., & van Dokkum, P. G. 2007, *ApJ*, 654, L107  
 Bremer, M. N., Jensen, J. B., Lehnert, M. D., Schreiber, N. M. F., & Douglas, L. 2004, *ApJ*, 615, L1  
 Bruzual, G., & Charlot, S. 2003, *MNRAS*, 344, 1000  
 Burgasser, A. J., Geballe, T. R., Leggett, S. K., Kirkpatrick, J. D., & Golimowski, D. A. 2006, *ApJ*, 637, 1067  
 Coe, D., Benítez, N., Sánchez, S. F., Jee, M., Bouwens, R., & Ford, H. 2006, *AJ*, 132, 926  
 Cole, S., Lacey, C. G., Baugh, C. M., & Frenk, C. S. 2000, *MNRAS*, 319, 168  
 Coleman, G. D., Wu, C. -, & Weedman, D. W. 1980, *ApJS*, 43, 393  
 Cooray, A. 2005, *MNRAS*, 364, 303  
 Cooray, A., & Milosavljević, M. 2005, *ApJ*, 627, L89  
 Cooray, A., & Ouchi, M. 2006, *MNRAS*, 369, 1869  
 Croton, D. J., et al. 2006, *MNRAS*, 365, 11  
 de Jong, R.S., et al. 2006, *The 2005 HST Calibration Workshop*, 121.  
 Dekel, A., & Birnboim, Y. 2006, *MNRAS*, 368, 2  
 Dickinson, M. 1998, *The Hubble Deep Field*, 219  
 Dickinson, M. 1999, *After the Dark Ages: When Galaxies were Young (the Universe at  $2 < Z < 5$ )*, 470, 122  
 Dickinson, M. et al. 2004, *ApJ*, 600, L99  
 Dickinson, M., & GOODS Team 2004, *Bulletin of the American Astronomical Society*, 36, 701  
 Dunkley, J., et al. 2008, *ApJS*, submitted, arXiv:0803.0586  
 Efstathiou, G., Ellis, R. S., & Peterson, B. A. 1988, *MNRAS*, 232, 431  
 Erb, D. K., Steidel, C. C., Shapley, A. E., Pettini, M., Reddy, N. A., & Adelberger, K. L. 2006, *ApJ*, 646, 107  
 Eyles, L. P., Bunker, A. J., Ellis, R. S., Lacy, M., Stanway, E. R., Stark, D. P., & Chiu, K. 2007, *MNRAS*, 374, 910  
 Ford, H. C., et al. 2003, *Proc. SPIE*, 4854, 81  
 Gabasch, A., et al. 2004, *A&A*, 421, 41  
 Giavalisco, M., et al. 2004a, *ApJ*, 600, L93  
 Giavalisco, M., et al. 2004b, *ApJ*, 600, L103  
 Granato, G. L., De Zotti, G., Silva, L., Bressan, A., & Danese, L. 2004, *ApJ*, 600, 580  
 Hathi, N. P., Malhotra, S., & Rhoads, J. E. 2008, *ApJ*, 673, 686  
 Iwata, I., Ohta, K., Tamura, N., Ando, M., Wada, S., Watanabe, C., Akiyama, M., & Aoki, K. 2003, *PASJ*, 55, 415  
 Iwata, I., Ohta, K., Tamura, N., Akiyama, M., Aoki, K., Ando, M., Kiuchi, G., & Sawicki, M. 2007, *MNRAS*, 376, 1557  
 Iye, M., et al. 2006, *Nature*, 443, 186  
 Kajisawa, M., et al. 2006, *PASJ*, 58, 951  
 Knapp, G. R., et al. 2004, *AJ*, 127, 3553  
 Kneib, J.-P., Ellis, R. S., Santos, M. R., & Richard, J. 2004, *ApJ*, 607, 697  
 Kron, R. G. 1980, *ApJS*, 43, 305  
 Labbé, I., Bouwens, R., Illingworth, G. D., & Franx, M. 2006, *ApJ*, 649, 67  
 Lee, K.-S., Giavalisco, M., Gnedin, O. Y., Somerville, R. S., Ferguson, H. C., Dickinson, M., & Ouchi, M. 2006, *ApJ*, 642, 63  
 Lehnert, M. D. & Bremer, M. 2003, *ApJ*, 593, 630  
 Madau, P., Pozzetti, L. & Dickinson, M. 1998, *ApJ*, 498, 106  
 Magee, D. K., Bouwens, R. J., & Illingworth, G. D. 2007, *Astronomical Data Analysis Software and Systems XVI*, 376, 261  
 Mannucci, F., Buttery, H., Maiolino, R., Marconi, A. & Pozzetti, L. 2007, *A&A*, 461, 423  
 Martin, D. C., et al. 2005, *ApJ*, 619, L59  
 Meurer, G. R., Heckman, T. M., & Calzetti, D. 1999, *ApJ*, 521, 64  
 Miyazaki, S., et al. 2002, *PASJ*, 54, 833  
 Mo, H. J., & White, S. D. M. 1996, *MNRAS*, 282, 347  
 Muñoz, J. A., & Loeb, A. 2008, *MNRAS*, submitted, arXiv:0711.2515  
 Oesch, P. A., et al. 2007, *ApJ*, 671, 1212  
 Oesch, P. A., et al. 2008, *ApJ*, submitted, arXiv:0804.4874  
 Oke, J. B., & Gunn, J. E. 1983, *ApJ*, 266, 713  
 Oppenheimer, B. D., & Davé, R. 2006, *MNRAS*, 373, 1265  
 Ouchi, M., et al. 2004a, *ApJ*, 611, 660  
 Ouchi, M., et al. 2004b, *ApJ*, 611, 685  
 Ouchi, M., Tokoku, C., Shimasaku, K., & Ichikawa, T. 2007, *Astronomical Society of the Pacific Conference Series*, 379, 47  
 Pelló, R., Schaerer, D., Richard, J., Le Borgne, J.-F., & Kneib, J.-P. 2004, *A&A*, 416, L35  
 Reddy, N. A., Steidel, C. C., Fadda, D., Yan, L., Pettini, M., Shapley, A. E., Erb, D. K., & Adelberger, K. L. 2006, *ApJ*, 644, 792  
 Reddy, N. A., Steidel, C. C., Pettini, M., Adelberger, K. L., Shapley, A. E., Erb, D. K., & Dickinson, M. 2007, arXiv:0706.4091  
 Rees, M. J., & Ostriker, J. P. 1977, *MNRAS*, 179, 541  
 Richard, J., Pelló, R., Schaerer, D., Le Borgne, J.-F., & Kneib, J.-P. 2006, *A&A*, 456, 861  
 Riess, A. G., et al. 2004, *ApJ*, 607, 665  
 Riess, A. G., et al. 2007, *ApJ*, 659, 98  
 Ryan, R. E., Jr., Hathi, N. P., Cohen, S. H., & Windhorst, R. A. 2005, *ApJ*, 631, L159  
 Sandage, A., Tammann, G. A., & Yahil, A. 1979, *ApJ*, 232, 352  
 Sawicki, M., & Thompson, D. 2006, *ApJ*, 642, 653  
 Scannapieco, E., & Oh, S. P. 2004, *ApJ*, 608, 62  
 Schaerer, D., Hempel, A., Pello, R., Egami, E., Richard, J., Kneib, J.-P., & Wise, M. 2007, *IAU Symposium*, 235, 425  
 Schiminovich, D., et al. 2005, *ApJ*, 619, L47  
 Sheth, R. K. & Tormen, G. 1999, *MNRAS*, 308, 119  
 Shimasaku, K., Ouchi, M., Furusawa, H., Yoshida, M., Kashikawa, N., & Okamura, S. 2005, *PASJ*, 57, 447  
 Silk, J. 1977, *ApJ*, 211, 638  
 Skinner, C. J., et al. 1998, *Proc. SPIE*, 3354, 2  
 Somerville, R. S., Lee, K., Ferguson, H. C., Gardner, J. P., Moustakas, L. A., & Giavalisco, M. 2004, *ApJ*, 600, L171  
 Spergel, D. N., et al. 2007, *ApJS*, 170, 377  
 Springel, V., et al. 2005, *Nature*, 435, 629  
 Stanway, E. R., Bunker, A. J., & McMahon, R. G. 2003, *MNRAS*, 342, 439  
 Stanway, E. R., Bunker, A. J., McMahon, R. G., Ellis, R. S., Treu, T., & McCarthy, P. J. 2004, *ApJ*, 607, 704  
 Stanway, E. R., McMahon, R. G., & Bunker, A. J. 2005, *MNRAS*, 359, 1184  
 Stanway, E. R., Bremer, M. N., Squitieri, V., Douglas, L. S., & Lehnert, M. D. 2008, *MNRAS*, in press, arXiv:0801.4559  
 Stark, D. P., Bunker, A. J., Ellis, R. S., Eyles, L. P., & Lacy, M. 2007a, *ApJ*, 659, 84  
 Stark, D. P., Ellis, R. S., Richard, J., Kneib, J.-P., Smith, G. P., & Santos, M. R. 2007b, *ApJ*, 663, 10  
 Stark, D. P., Loeb, A., & Ellis, R. S. 2007c, *ApJ*, 668, 627  
 Steidel, C. C., Adelberger, K. L., Giavalisco, M., Dickinson, M. and Pettini, M. 1999, *ApJ*, 519, 1  
 Strolger, L.-G., et al. 2004, *ApJ*, 613, 200  
 Szalay, A. S., Connolly, A. J., & Szokoly, G. P. 1999, *AJ*, 117, 68

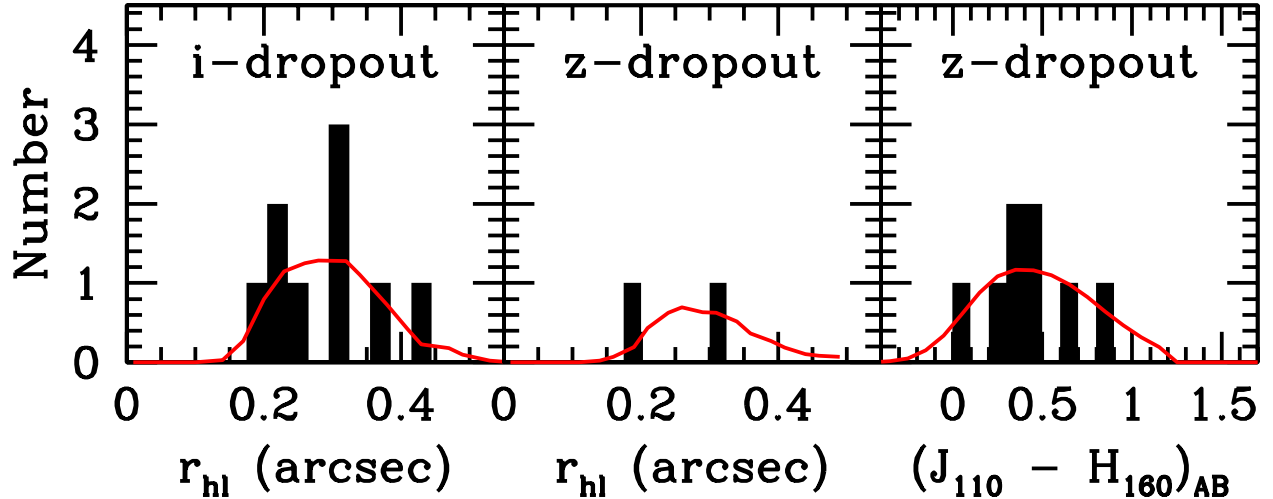


FIG. A1.— Comparison between the observed properties of the  $i$  and  $z$  dropouts (black histogram) and that expected based on our model for star-forming galaxies at  $z \gtrsim 6$  (red lines: see §4 and Appendix B for a description of this model). The leftmost panels show comparisons between the observed and expected half-light radii ( $r_{hl}$ ) while the rightmost panel shows comparisons between the observed and expected  $UV$  colors. Only galaxies brightward of  $H_{160,AB} = 26.4$  and  $H_{160,AB} = 27.0$  in our HUDF and NICPAR selections are included in the distribution of half-light radii. This leaves us with some leverage in examining the size (surface brightness) distribution. Otherwise, selection effects would tend to dominate, excluding all the larger sources from these comparisons and we would be left with only those sources whose sizes were very similar to that of the PSF. For the comparisons we make involving  $UV$  colors, all search fields are considered. In general, good agreement is found between the observed and expected properties, providing us with a reasonable amount of confidence in the model we are using to calculate the effective selection volumes for star-forming galaxies at  $z \gtrsim 7$ .

Thompson, R. I., Rieke, M., Schneider, G., Hines, D. C., & Corbin, M. R. 1998, ApJ, 492, L95  
 Thompson, R. I., Storrie-Lombardi, L. J., Weymann, R. J., Rieke, M. J., Schneider, G., Stobie, E., & Lytle, D. 1999, AJ, 117, 17  
 Thompson, R. I., et al. 2005, AJ, 130, 1  
 Trenti, M., & Stiavelli, M. 2008, ApJ, 676, 767  
 Wang, B., & Heckman, T. M. 1996, ApJ, 457, 645  
 Wiklind, T., Dickinson, M., Ferguson, H. C., Giavalisco, M., Mobasher, B., Grogin, N. A., & Panagia, N. 2007, in press, arXiv:0710.0406

Wyder, T. K., et al. 2005, ApJ, 619, L15  
 Wyithe, J. S. B., & Loeb, A. 2006, Nature, 441, 322  
 Yan, H. & Windhorst, R. A. 2004, ApJ, 612, L93  
 Yan, H., et al. 2005, ApJ, 634, 109  
 Yang, X., Mo, H. J., & van den Bosch, F. C. 2003, MNRAS, 339, 1057  
 Yoshida, M., et al. 2006, ApJ, 653, 988

## APPENDIX

### A. LARGE SCALE STRUCTURE UNCERTAINTIES

In this work, we derived our best-fit LF at  $z \sim 7$  by comparing the observed surface density of galaxies with what we would expect based on a model LF and then maximizing the likelihood of the model LF. We assumed Poissonian statistics in computing the likelihood of various model LFs (§4). Our decision to adopt a Poissonian model in computing these likelihoods rather utilizing a more conventional approach like SWML was to take advantage of the substantial amount of deep, wide-area near-IR imaging (e.g., the ISAAC or MOIRCS data) we have to constrain the  $UV$  LF at  $z \sim 7$ . Since most of these imaging data contain no  $z \sim 7$  candidates, we would not be able to use that data for improving our determination of the  $UV$  LF at  $z \sim 7$ , had we chosen to use the conventional SWML or STY79 techniques. However, modelling our observational results using Poissonian statistics (and assuming no large-scale structure variations), we are able to take advantage of this information to constrain the shape of the  $UV$  LF.

Of course, in modelling the observational results using this approach, we are inherently assuming that the volume density of high-redshift star-forming galaxies is statistically homogeneous across the sky. In reality, however, the distribution of galaxies is modestly clustered, and therefore the mean volume density of galaxies will show significant variations as a function of position. These variations in the mean density occur as a result of large-scale structure and will have an effect on the best-fit  $UV$  LF we derive at  $z \sim 7$ , scattering it away from the cosmic average.

To estimate the effect that such variations will have on our fit results, we ran a set of Monte-Carlo simulations. We varied the surface density of model dropouts in each of our search fields by  $\sim 30\%$  RMS (see §4.1) and then recomputed the  $UV$  LF in the same way as in §4.2. We found  $1\sigma$  variations of  $\pm 0.1$  mag in the values of  $M_{UV}^*$  and  $\pm 30\%$  in the values of  $\phi^*$  at  $z \sim 7$ . Adding these uncertainties in quadrature with those deriving from Poissonian uncertainties (§4.2), the total uncertainty in  $\phi^*$  at  $z \sim 7$  is 0.4 dex and  $M_{UV}^*$  is  $\pm 0.4$  mag.

The effect of large-scale structure variations on the constraints we place on the  $UV$  LF at  $z \sim 9$  is much smaller in general. Given that we have no sources in our  $J$ -dropout sample, the Poissonian uncertainties ( $\pm \sim 100\%$ ) dominate over the expected field-to-field variations, which are  $\pm \sim 20\%$  (see §4.2 or Bouwens et al. 2005).

## B. PLAUSIBILITY OF OUR MODEL FOR ESTIMATING THE SELECTION VOLUMES OF DROPOUT SAMPLES AT $Z \gtrsim 7$

Besides small number statistics, perhaps the biggest uncertainty in the present determination of the rest-frame  $UV$  LF at  $z \gtrsim 7$  is in our estimates of the selection volumes for the two dropout samples. We derived these estimates using the following model for the sizes, morphologies, and  $UV$  colors of galaxies at  $z \gtrsim 7$ . We assumed that star-forming galaxies at  $z \gtrsim 7$  have similar pixel-by-pixel profiles to the  $z \sim 4$   $B$ -dropouts in the HUDF, but with physical sizes scaled by a factor of  $(1+z)^{-1.1}$  (e.g., at  $z \sim 7$  galaxies of a given luminosity have approximately half the physical size of star-forming galaxies at  $z \sim 4$  and therefore four times the surface brightness). The  $UV$ -continuum slopes  $\beta$  were taken to have a mean of  $-2.0$  and  $1\sigma$  scatter of  $0.5$ . Both assumptions were chosen to match the trends found in the observations from  $z \sim 6$  to  $z \sim 2$  for the sizes (e.g., Bouwens et al. 2006; Bouwens et al. 2004a; Ferguson et al. 2004) and colors (Stanway et al. 2005; Bouwens et al. 2006).

Of course, just because the present model is a reasonable extrapolation of the trends (in sizes and colors) found at lower redshift does not mean it will accurately represent star-forming galaxies at  $z \gtrsim 7$ . Therefore, it makes sense for us to compare this model with the limited data on  $z \gtrsim 6$  galaxies where they exist. We begin by comparing the observed  $J - H$  colors of  $z$ -dropouts in our sample with that predicted using our best-fit LF ( $\phi \sim 0.0011 \text{ Mpc}^{-3}$ ,  $M_{1900,AB}^* \sim -19.8 \text{ mag}$ ,  $\alpha \sim -1.74$ ) and the model we just described above (see also §4) for calculating the selection volumes. We include the comparison in the rightmost panel of Figure A1.

Similarly, we can compare the half-light radii of  $z$ -dropouts in our sample with that predicted from our models. To ensure that the size distribution we derive for  $z$ -dropouts is not dominated by surface brightness selection effects (which only allows for the selection of point-like sources near the magnitude limit), we only consider the sizes of  $z$ -dropouts that are  $\gtrsim 0.7 \text{ mag}$  brighter than the magnitude limit. Unfortunately, this only leaves us with  $\sim 2$  galaxies for making this comparison. The result is shown in the middle panel of Figure A1. The model predictions appear to be in reasonable agreement with the observations. As one additional check on the size-redshift scaling we are using to model the sizes (surface brightnesses) of  $z \sim 7$  galaxies, we also include a comparison of our model predictions with the half-light radii of  $z \sim 6$   $i$ -dropouts in our search fields (leftmost panel of Figure A1).

## C. COMPARISON WITH THE RICHARD ET AL. (2006) RESULTS

In the present work (e.g., §5.1 or Table 7), we found a significantly smaller (i.e.,  $\sim 1/18$ ) volume density of galaxies at the bright end of the  $UV$  LF at  $z \gtrsim 7$  than has been inferred at  $z \sim 4$  (e.g., Steidel et al. 1999; Reddy et al. 2007; Bouwens et al. 2007). This is in significant contrast with the volume densities of  $z \gtrsim 6$  galaxies inferred by Richard et al. (2006) from searches for  $z$  and  $J$  dropouts in  $\sim 12 \text{ arcmin}^2$  of deep ( $\sim 24.5 \text{ AB mag}$  at  $5\sigma$ ) near-IR data behind two low-redshift lensing clusters Abell 1835 and AC114. Richard et al. (2006) found 13 first and second category  $z$  and  $J$  dropouts in their search that they consider plausible  $z > 6$  galaxies. Modelling the lensing amplification, contamination, and overall incompleteness of their search, Richard et al. (2006) estimated the  $UV$  LFs at  $z \sim 6 - 8$  and  $z \sim 8 - 10$ . In significant contrast to our results, the volume density of bright galaxies in the Richard et al. (2006) LFs were found to be very similar to what has been found at  $z \sim 3 - 4$  (i.e., Steidel et al. 1999; Bouwens et al. 2007).

What is the reason for these substantial differences? While one possible explanation could be “cosmic variance” (i.e., field-to-field variations), simple estimates for the variance one expects in the volume density of high-redshift sources behind a typical cluster is of order  $\sim 50\%$  RMS, and therefore much smaller than the factor of  $\gtrsim 10$  differences seen here. These “cosmic variance” estimates assume a pencil beam geometry, a redshift window of width  $\Delta z = 1$ , an angular diameter of  $\sim 30 \text{ arcmin}^2$ , and a bias of  $\sim 7$ , which is appropriate for galaxies at  $z \sim 7$  with a volume density of  $\sim 10^{-3.5} \text{ Mpc}^{-3}$  (see also Somerville et al. 2004; Trenti & Stiavelli 2008).

Instead a much more probable explanation for the discrepancy seen here is simply that a substantial fraction of the Richard et al. (2006)  $z \gtrsim 6$  candidates are spurious in nature. After all, none of their best candidates were detected at significance levels much higher than  $2.5\sigma$ , making each of the candidates in their sample open to question. Clearly, given the area of empty sky within their  $12 \text{ arcmin}^2$  search area, it would not be difficult to imagine a small number of these empty areas of sky showing large enough positive fluctuations to satisfy their detection thresholds just by chance! To their credit, Richard et al. (2006) recognized the significance of this concern and attempted to model this effect. After extensive Monte-Carlo simulations, they argued that the number of dropouts found in their samples significantly exceeded that expected from the noise. Unfortunately, such techniques can be highly sensitive to even the smallest errors in the noise model, and therefore it is not entirely clear how much weight we should give to the simulations Richard et al. (2006) have run to control for this process.

A much more straightforward and robust way of estimating the spurious fraction is to look at their candidates in deeper near-IR data (as Bremer et al. 2004 used to evaluate the reality of the Pelló et al. 2004  $z \sim 10$  candidate). Such data are available for two deep  $\sim 0.7 \text{ arcmin}^2$  NIC3  $H_{160}$  exposures over each of their two clusters (AC114 and Abell1835). These NICMOS pointings reach to  $\sim 26.8 \text{ AB mag}$  ( $5\sigma$ ),  $\sim 2 \text{ mag}$  deeper than the ISAAC data used by Richard et al. (2006) in their searches. These pointings provide very deep  $H_{160}$ -band coverage for 2 first and second category  $z \gtrsim 6$  candidates reported by Richard et al. (2006) and 5 first, second, and third category candidates. The first and second category candidates of Richard et al. (2006) were the  $z \gtrsim 6$  candidates to which they ascribed the highest confidence while the third category candidates were ascribed slightly lower confidence. Of the 5 such candidates with very deep  $H_{160}$ -band coverage, none show up at  $> 2\sigma$  significance, strongly arguing that a substantial fraction of their candidates do not correspond to real sources. Taken by itself, it implies that  $\gtrsim 80\%$  of the Richard et al. (2006) first, second, and third category  $z \gtrsim 6$  candidates are spurious (68% confidence). If we only consider first and second

category candidates (the highest confidence candidates) with deep NICMOS data, the NICMOS non-detections imply that  $\gtrsim 56\%$  of the Richard et al. (2006) candidates are spurious (68% confidence).

We also do not find it particularly encouraging that none of the dropout candidates in the Richard et al. (2006) sample are detected in the deep IRAC  $3.6\mu$  imaging which exist around these clusters (Schaerer et al. 2007). There are six sources in the Richard et al. (2006) sample which are sufficiently isolated from the neighbors for these upper limits to have particular significance. Given the reported  $H$ -band magnitudes of the Richard et al. (2006)  $z \gtrsim 7$  candidates (ranging from 24.6 to 25.2 AB mag), we would suspect it should be easy to detect these sources in the very deep IRAC data available (reaching to 25.8 AB mag at  $2\sigma$ ), especially given that typical  $(z_{850} - 3.6\mu m)_{AB}$  colors for other  $z \sim 6 - 8$  candidates range from  $-0.5$  mag to  $1.5$  mag (Yan et al. 2006; Labbé et al. 2006; Eyles et al. 2007; Bradley et al. 2008). While Schaefer et al. (2007) suggest that the IRAC non-detections argue for a very young population, we do not think the candidates' reality is well enough established to draw any conclusions about the properties of the purported sources. Rather we find it worrying that none of the available NICMOS or IRAC data over these clusters have provided us with evidence that any of the Richard et al. (2006) candidates are real!

Finally, we note the overall prevalence of  $z \gtrsim 6$  candidates found by Richard et al. (2006) behind AC114 and Abell 1835 is at least  $\gtrsim 10\times$  higher than found in searches around other lensing clusters with much deeper, higher quality NICMOS data. Bouwens et al. (2008) have quantified this by examining the deep ( $\gtrsim 26.5$  AB mag at  $5\sigma$ )  $J$  and  $H$ -band imaging data around 6 galaxy clusters (CL0024, MS1358, Abell 2218, Abell 2219, Abell 2390, Abell 2667) and the deep ( $\gtrsim 26$  AB mag at  $5\sigma$ )  $J$ -band imaging around three other galaxy clusters (Abell 1689, Abell 1703, 1E 0657-56). In total, the deep near-IR imaging data around these clusters cover  $\gtrsim 20$  arcmin<sup>2</sup> in total, almost double what was considered in Richard et al. (2006) and extending some  $\gtrsim 1 - 2$  mag deeper. Only one  $z \gtrsim 7$  candidate (i.e., A1689-zD1: Bradley et al. 2008) and one  $z \sim 6.5$  candidate (Kneib et al. 2004) is found over these fields to the same magnitude limit (i.e., 25.5 AB mag) as is considered in the Richard et al. (2006) search. This is to be compared with 13 first and second category  $z \gtrsim 6$  candidates found by Richard et al. (2006) in a search over just half the area. Since it seems unlikely that high-redshift dropouts are  $\gtrsim 10\times$  more common behind the two particular clusters considered by Richard et al. (2006) than the 9 other clusters with deep NICMOS data, this again suggests that the majority (i.e.,  $\gtrsim 90\%$ ) of the  $z \gtrsim 6$  candidates found in the Richard et al. (2006) search are simply spurious sources.

#### D. $Z \gtrsim 7$ DROPOUTS IN PREVIOUS SAMPLES NOT IN CURRENT SELECTIONS

There were a small number of candidates in our previous samples (3  $z$ -dropout candidates from Bouwens et al. 2004c and 3  $J$ -dropout candidates from Bouwens et al. 2005) which did not make it into our current selections. In this section, we describe why those particular candidates are not included in our current selections.

Let us first consider the three  $z$ -dropout candidates from the HUDF (Bouwens et al. 2004c) which do not make it into our current samples. As has already been discussed in Bouwens & Illingworth (2006) and Labbé et al. (2006), two of those candidates (UDF-818-886 and UDF-491-880) were the direct result of the ‘‘Mr. Staypuft’’ anomaly (Skinner et al. 1998), which produces faint electronic ghosts 128 pixels from bright stars. Since the ‘‘Mr. Staypuft’’ anomaly is now carefully modelled and explicitly removed in our ‘‘nicred.py’’ reductions (Magee et al. 2007), this anomaly should not pose a problem for our current selections. The third candidate (UDF-825-950) may still be a high-redshift star-forming galaxy, but did not match the S/N thresholds used for the current selection.

Now we consider the three  $J$ -dropout candidates reported by Bouwens et al. (2005). What became of these three candidates? Two of the three candidates (UDFNICPAR1-04151142 and UDFNICPAR2-09593048) show detections in the ultra-deep  $V$ -band imaging recently taken over the NICMOS parallels to the HUDF and therefore are clearly not  $z \sim 9 - 10$  galaxies. The other candidate (UDFNICPAR1-05761077) is not detected at high enough significance in our current reductions of the NICMOS parallels to the HUDF and appears to have been spurious. Spurious sources are a particular concern over the NICMOS parallels to the HUDF given the minimal amounts of dithering used in acquiring the data. Therefore, substantial care has been taken to accurately characterize the read-out properties of individual pixels and correct for any pixel-by-pixel detector (or reduction) signatures (see §2.1).

The loss of these three  $z \sim 9 - 10$   $J$ -dropout candidates from our samples should not be a significant cause for concern. In the Bouwens et al. (2005) analysis, the emphasis was on setting an *upper limit* on the volume density of  $UV$ -bright  $z \sim 9 - 10$  galaxies and therefore we tried to err on the side of *including* candidates in our samples if there was any uncertainty about their nature.